

BIRZEIT UNIVERSITY
FACULTY OF INFORMATION TECHNOLOGY

***Position Control of Shape Memory Alloy
(SMA) Wire Using Model- and Behavioral-
based and Non Model-based Controllers***

A THESIS
SUBMITTED AS PARTIAL FULFILLMENT
OF THE REQUIREMENTS

for the degree

MASTER OF SCIENTIFIC COMPUTING

By

Samah A. M. Ghanem

Supervisors

**Dr. Hassan Shibly,
Birzeit University,
Ramallah, Palestine**

**Univ.-Prof. Dr.-Ing. Dirk Söffker,
University of Duisburg-Essen,
Duisburg, Germany**

December, 2008

***Position Control of Shape Memory Alloy
(SMA) Wire using Model- and Behavioral-
Based and Non Model-Based Controllers***

By

Samah A. M. Ghanem

This Thesis was defended successfully On 7-05-2009 and approved by :

Committee Members

Signature

- | | | |
|----|--|-------|
| 1. | Dr. Hassan Shibly | |
| 2. | Univ.-Prof. Dr.-Ing. Dirk Söffker | |
| 3. | Dr. Ibrahim Hammad | |
| 4. | Dr. Yousef Alsweity | |
-

Dedication

“To my Mother”

Acknowledgement

I would like to thank Dr. Hassan Shibly and Prof. Dirk Soeffker my supervisors for their support and follow-up of every step in my work, and for helping me to proceed the work smoothly. I would like to express my deep gratitude for opening the doors of the labs of Dynamics and Control at SRS, University of Duisburg-Essen, Germany for me, and for giving me all the resources and facilities required. I would also like to thank Prof. Soeffker's team for the help they offered to me during my work and for the support they all give during my stay and especially Dr. Wend, Mr. Saadawia, Mrs. Liu, and Mr. Özbek. Thanks to Birzeit University which makes the life easy for its students by evaluating the course of my study in Germany as a regular local course.

TABLE OF CONTENTS

Dedication	iii
Acknowledgment	iv
III.....	Dedication
IV.....	Acknowledgement
VI.....	List of Tables
VI.....	List of Figures
VII.....	Abstract

<i>Chapter 4</i>	
Non Model-Based Control of SMA	31
4.1. Introduction	31
4.2. PID Controller	31
4.2.1. PI Position Control Experimental results	32
4.3. Adaptive Control	35
4.3.1. MRAC Control	35
4.3.2. STC Control	35
4.3.3. Designing the PID Adaptive Controller	36
4.3.4. Experimental Results	42
4.4. Conclusions on the non model-based approach	49
 <i>Chapter 5</i>	
Results and Conclusion	51
5.1. Conclusion	51
5.2. Motivation and Future Work	52

<i>Reference</i>	53
APPENDIX- A <u>SOFTWARE AND MATLAB CODE</u>	<u>57</u>
APPENDIX- B <u>SIMULINK MODELS</u>	<u>63</u>
APPENDIX-C <u>TABLES AND FIGURES</u>	<u>74</u>

List of Tables

Table 2.1. The parameters of the NiTi Shape Memory Alloy.

List of Figures

- Figure 1.1 SMA Phase Transformations Elongation.
- Figure 1.2 Elongation versus Temperature; Hysteresis in SMA.
- Figure 2.1. Experimental Hardware and Software Blocks.
- Figure 2.2. The SMA Test Rig.
- Figure 2.3. Flow of signals in the experimental setup.
- Figure 3.1. Schematic Diagram of the Behavioral-Based Feedforward Controller Main Blocks.
- Figure 3.2. The Austinite Model Feedforward and PI Controller
- Figure 3.3. The Martensite Model Feedforward and PI Controller
- Figure 3.4. The AM Model Feedforward and PI Controller

- Figure 3.5. Austinite, Martensite, and AM models results in feedforward with PI controllers.
- Figure 3.6. The V-Model Feedforward and PI Controller
- Figure 3.7. V-Model results in Feedforward with PI controllers with signal generator as input.
- Figure 3.8. The O-Model Feedforward and PI Controller
- Figure 3.9. O-Model results working as a feedforward controller.
- Figure 4.1. PID Controller.
- Figure 4.2. The PI Controller for position control of the SMA.
- Figure 4.3. PI Position Controller Results.
- Figure 4.4. MRAC adaptive control system.
- Figure 4.5. STC adaptive control system.
- Figure 4.6. MRAC system for a first order plant.
- Figure 4.7. Adaptive controller based on adaptation law (4.4).
- Figure 4.8. The PID Adaptive controller combined MRAC and STC.
- Figure 4.9. PID Adaptive controller for position control of the SMA.
- Figure 4.10. Adaptive Controller in (4.4) result with $\gamma = 1$.
- Figure 4.11. Enhanced PID Adaptive Controller results, all adaptive PID parameters signal vector is the error signal result with $\gamma = 1$.
- Figure 4.12. PID Adaptive Controller, with $\gamma = 1$.
- Figure 4.13. PID Adaptive Position Controller Results with $\gamma = 1$.
- Figure 4.14. PI and PID adaptive controller's results using chaotic signal as the desired position.
- Figure 4.15. Position Control Error of PI and PID adaptive controller under different frequencies of the desired position.

Abstract

Shape Memory Alloys exhibit a hysteretic shape memory behavior under heating and cooling conditions. The purpose of this research work is to develop a control algorithm to control the position of the SMA wire actuator. The first scope of experiments was to test and to model the SMA behavior through model and behavioral-based control. Firstly, an Austinite-Martensite-model (AM-model) is derived from the heat transfer function substituting the change in the SMA length of the resistance equation for the austinite subsystem while other assumptions for the change in the material from a passive to an active element to build the martensite subsystem, the model was tested by comparing the behavior of the model with the behavior of the

experiment, therefore a feedforward control structure was used. Secondly, a Volume-model (V-model) is derived from the heat transfer function taking the change in the volume in the SMA wire under heating and cooling transformations, the model is tested in a feedforward controller. Thirdly, the Ohm-model (O-model) is derived from the previous research work [1] evaluating the change in resistance in different phase transformations to find the excitation current through Ohms law, the model is tested for feedforward control. All these model- and behavioral-based approaches are not able to control the position of the SMA wire due to their strong temperature dependency; where the temperature of the wire cannot be measured by a sensor as it is not equal in all points of the wire's surface, while the computation time in the calculations of the approximated wire temperature using the heat transfer equation doesn't match the real time needs of the system. The second scope of experiments covers a non model-based control using a PI controller and an PID adaptive controller and they both have excellent performance in the position control of the SMA wire, the control error increases at high frequencies due to low response time of the material at

natural cooling. The outcome of this research work; firstly, a strong understanding of the material capabilities as it is not based on theoretical work and simulations but on real experimental environment where methods can be validated. Secondly, a robust SMA PI tuned position controller. Thirdly, an adaptive controller that can be used to tune the coefficients of the SMA wire or any plant with unknown parameters, the advantage is that non model-based controllers are not temperature dependant, and they just need few tuning of the system procedures. However, this research provides a basis for planning applications of the material in mechanical based engineering systems like in Smart Antennas, or in automated devices, etc. While encourages continuous research in the modelling part of the SMA to have a general behavioral-model based on the material characteristics. All the experiments are tested using

an NiTi SMA wire. Using MATLAB/SIMULINK 6.1/5.0 and the dSPACE DS1104 data acquisition real time system.

Chapter 1

Introduction

Shape Memory alloy wires are wires composed of different set of materials that have a shape memory behavior under temperature changes. Such type of behavior is identified as a hysteretic behavior. The usage of the shape memory behavior of the SMA in different applications especially as actuators requires control algorithms that can predict and control the SMA using a model for forecasting and prediction of the behavior of the SMA. So, the objective of this research work is to build this control algorithm for the SMA wire to control its position. The SMA wire forms the actuator plant in the control loop. Different theoretical approaches and experimental results based on a non model- based and a model and behavioral- based control approaches for the position control of the SMA will be introduced.

All controller models are built in SIMULINK and tested with the SMA test rig using real time SIMULINK workshop and the dSPACE real time control box at the SRS labs in the University of Duisburg-Essen in Germany. Model- and behavioral- based approaches were tested by comparing the behavior of the model with the behavior of the experiment i.e. in a feedforward control structure. The non model- based approach introduces two different ways of control which is the PI and the PID adaptive control.

This chapter will introduce the SMA in more details; the phase transformations of the material under temperature changes, and the set of different applications the SMA is used in. Chapter 2 will describe the experimental setup of the software and hardware components used in the experiments, and a set of experimental results will be introduced for the hysteretic behavior of the SMA under different parameter changes like constant load, amplitude and frequency of the excitation signal which will be appended in appendix C. The MATLAB code used to calculate the approximated temperature versus elongation of the wire is appended in appendix A. Chapter 3 will introduce different ideas tested to build a model- based control system using the heat transfer equations and other behavioral assumptions. Models built in SIMULINK are

appended in appendix B. Chapter 4 will introduce an introduction about PID control and adaptive control and its different approaches, the models mathematical derivation and block diagrams are mentioned. The results of successful PI and PID adaptive control will be introduced and a comparison to evaluate both control schemes is done in terms of controller performance to low and high input frequencies of the desired position. The conclusions will lead to motivation and future work in the SMA material research and applications in Chapter 5.

1.1. SMA Material

Shape Memory Alloy (SMA), also called smart materials has characteristics of normal metals but their behavior is different under the change of temperature; whether this temperature change is external or by electrical heating. Unlike normal conductors, it contracts by heating and expands by cooling. This hysteretic behavior encourages scientists to try to build models for the SMA to model the hysteretic behavior of the metal based on different material characteristics. Some of these studies are differential hysteresis modeling of SMA [2], thermodynamic model of SMA [3], modeling and simulation of SMA [4], thermomechanical model of SMA using Prandtl-Ishlinskii hysteresis model [5], and a mathematical model-based on experimental data [6].

Additive to the hysteretic behavior or shape memory effect, the SMA has other characteristics; its pseudo elasticity, corrosion resistance, and high load to weight ratio which are needed in engineering appliances. However, this makes it also a candidate for biomedical and aerospace appliances.

1.2. Applications of SMA

SMA is used in a wide range of applications. The different doping of the shape memory alloy using different materials leads to different characteristics of the alloy; making it suitable for different applications in different industries. Some examples of these alloys are Ag-Cd, Au-Cd, Cu-Al-Ni, Cu-Sn, Cu-Zn-(X), In- Ti, Ni-Al, Ni-Ti, Fe-Pt, Mn-Cu, and Fe-Mn-Si. Examples of its usage in different industries; in the biomedical industry;

in bone plates; where memory effect pulls bones together to allow healing, and in surgical anchor; when healing progresses, muscles grow around the wire preventing tissue damage that could be caused by staples or screws. In aerospace, as actuators in planes; electric signals are sent through the wires to allow precise movement of the wings. Other applications such as super elastic glasses, household appliances, robots, etc. [25, 26].

1.3. Hysteresis in SMA

Hysteresis behavior of the SMA is experienced under heating and cooling conditions which is the shape memory effect discovered in certain copper alloys during the 1950s and then found in nickel titanium (NiTi) [9]. This explains the reason behind the naming of these materials as shape memory alloys as they keep a memory of the last shape they were in, returning to their saved shape under a certain trigger either a temperature decrease i.e. cooling or an external stress. This type of behavior can be used in different kind of applications as an actuator in different engineering systems.

The SMA exhibits two main phase transformations: The austenite phase or the A-phase, and the martensite phase or the M-phase. Another minor precursor phase called the R-phase that occurs in the SMA before the start of the main phase transformation on heating and cooling, while it can be suppressed by heat treatment of the material, this phase is out of the scope of this research [1, 7, 8]. The different characteristics of the material under different phase transformations in its electrical resistivity and the young modulus, etc. could help in specific applications and also in feedback control of SMA actuators [9].

The high temperature phase transformation is called the austenite, and the low temperature phase is called the martensite [7]. When martensite, the less symmetric deformed phase, is heated it begins to structurally change into austenite, the highly symmetric un-deformed phase, at the austenite start temperature (A_s). This phase change is completed at the austenite finish temperature (A_f). Similarly, when austenite

is cooled it begins to change into martensite at the martensite start temperature (M_s) and finishes the transformation at the martensite finish temperature (M_f) [10].

The different shapes of the SMA surface at different phase transformations is shown in figure 1.1. The changes in the length of the SMA, the shift of the atoms and their corresponding change in the bond's shape leads to several differences in the properties of the austenitic and martensitic phases of the material.

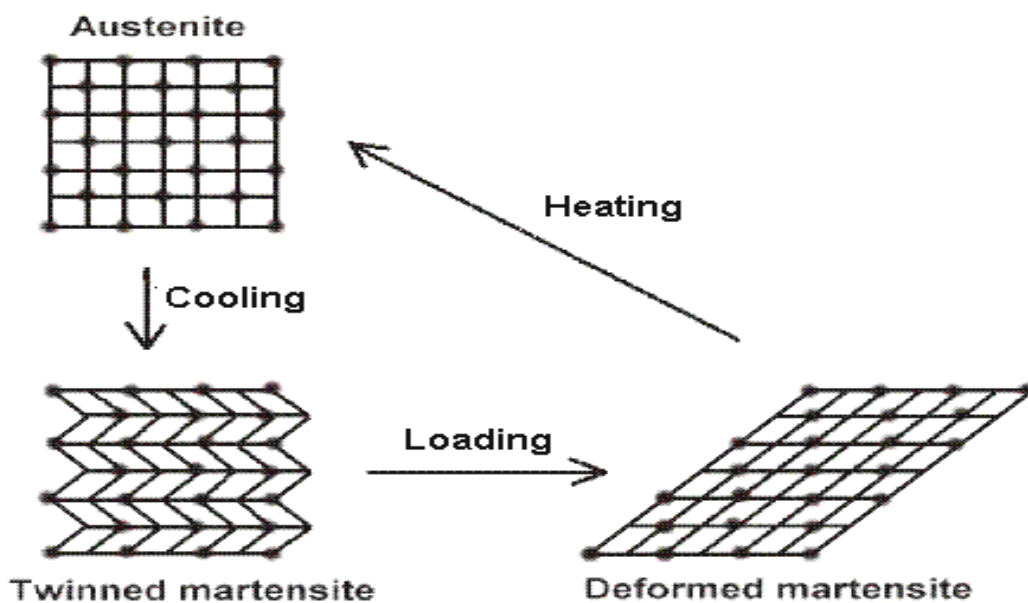


Figure 1.1. SMA Phase Transformations. Heating the SMA leads to Austenite cubic shape, cooling leads to a Twinned martensite, loading leads to the Deformed martensite [25].

The hysteretic behavior is shown in figure 1.2 [11]. The difference between these temperatures is called the hysteresis band. This figure shows a clean one hysteresis cycle while experiments show multiple hysteretic regions in a single hysteresis cycle under repetitive excitation cycles. See figure C2.2, appendix C. The actuation frequency of the SMA material is defined by the response time of the material to move from its maximum contraction limit at austenite final temperature A_f to its maximum expansion limit at martensite maximum temperature M_f ; i.e. to obtain a hysteresis cycle.

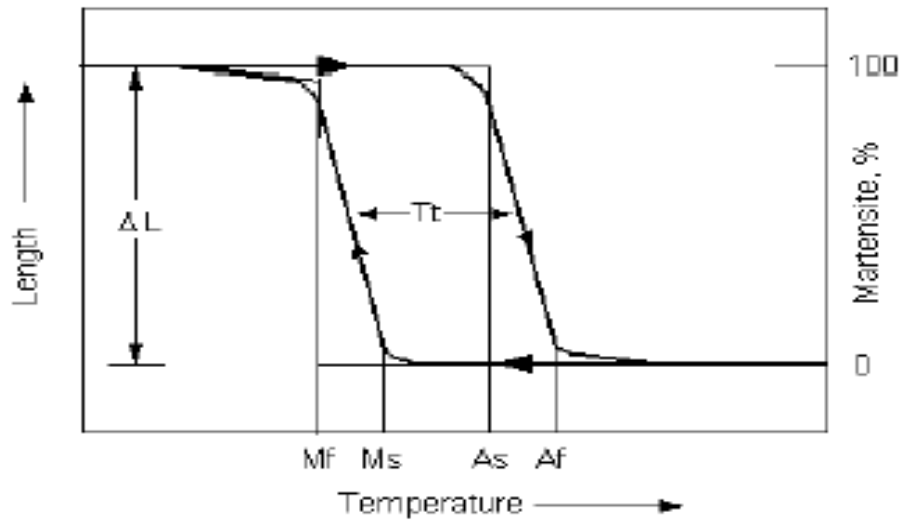


Figure 1.2 Elongation versus Temperature; Hysteresis in SMA. Hysteresis bandwidth is defined as T_t and phase transformation temperatures for austinite and martensite are shown [11].

1.3.1. The Austinite Phase

The austinite phase is the SMA material state exhibited at high temperature. Under heating conditions, normally electrical heating the SMA wire changes its structure into the austinite cubic strong structure where the contraction of the wire length begins at A_s and ends to its maximum limit at A_f . Each SMA has its own measured experimental values for A_s and A_f .

1.3.2. The Martensite Phase

The martensite phase is the SMA material state exhibited at low temperature or external stress. Under cooling conditions, normally natural cooling, the material is called twinned martensite and under stress it's called a deformed martensite. The SMA wire changes its structure to an elastic structure causing an expansion in the wire length which starts at M_s and its maximum limit ends at M_f . Each SMA has its own measured experimental values for M_s and M_f .

Chapter 2

Experimental Setup

2.1. Introduction

The experimental setup includes all the hardware and software components used to run the experiments, it includes the SMA test rig, power supplies, a PC with installed MATLAB/SIMULINK, and a dSPACE control box hardware and software.

Figure 2.1 shows the experimental setup with all connected blocks [12].

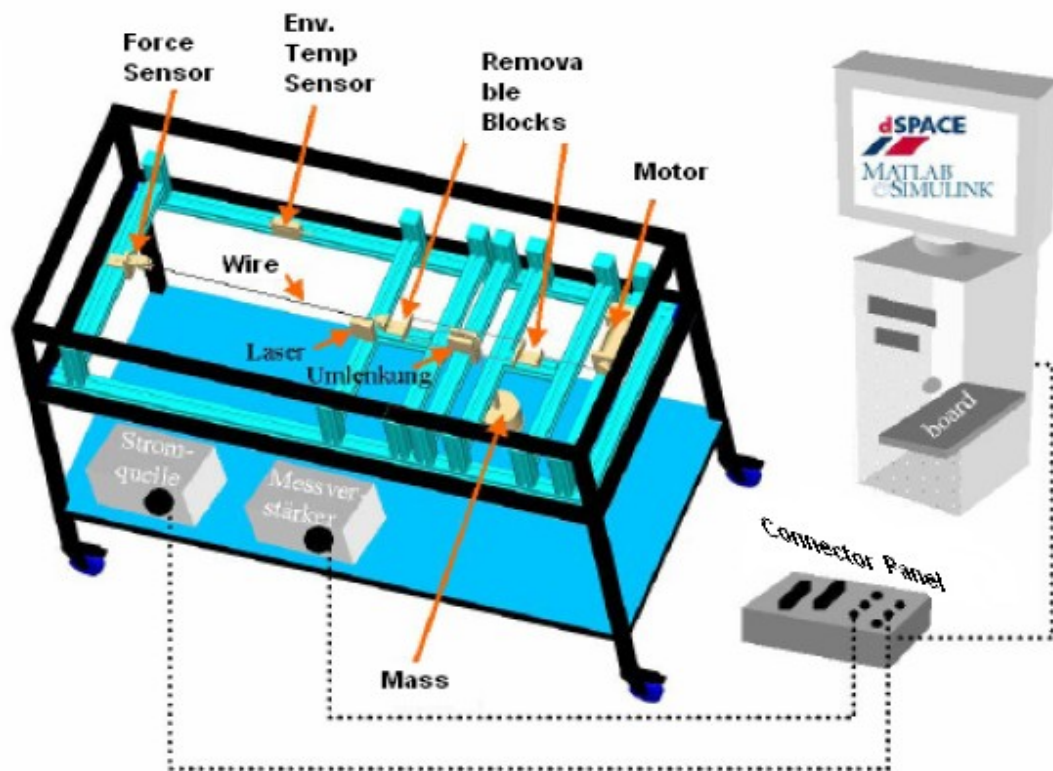


Figure 2.1. Experimental Hardware and Software Blocks [12].

The set of experiments done includes two scopes; the first scope of experiments was to examine the hysteresis behavior of the SMA changing different parameters, similar to the work done in [13]. While the second scope of experiments were done for the purpose of building a position controller of the SMA wire. In this research, a single NiTi SMA is considered.

2.2. SMA Test Rig

The SMA Test Rig includes all the hardware required for the experiment: The NiTi SMA wire, a constant load connected to the wire, a slider or a removable block to enable the movement of the wire and the connected mass under negative and positive elongations, and a DC motor that was connected for dynamic loads but it was disconnected and wasn't used in the control experiments. The SMA wire used in the experiments is a Nickel Titanium wire, with the parameters mentioned in Table 2.1. Other variables used for the SMA are in Table C.1, appendix C .

Length (m)	Radius (m)	Density (Kg/m ³)	Area (m ²)	Volume (m ³)
0.55	0.0002	6500	$6.9115 \cdot 10^{-4}$	$6.9115 \cdot 10^{-8}$

Table 2.1. The parameters of the NiTi Shape Memory Alloy.

Three sensors were connected to the test rig; a force sensor to measure the force input to the system, an environment temperature sensor, and a laser sensor that's used to measure the position of the SMA wire. The test rig is also connected to a power supply that feeds the wire with the current needed to perform the heating. The maximum input current is 2A limited by saturation SIMULINK blocks to 1.7A. The maximum input voltage is -10, +10 Volts to the dSPACE that will be discussed in the next section.

Figure 2.2 shows the SMA test rig at the Dynamics and Control labs ,SRS, at University of Duisburg-Essen in Germany. Figures of the SMA test rig and all its connections and interfaces to power supply and dSPACE control panel can be found in figure C.1, appendix C.

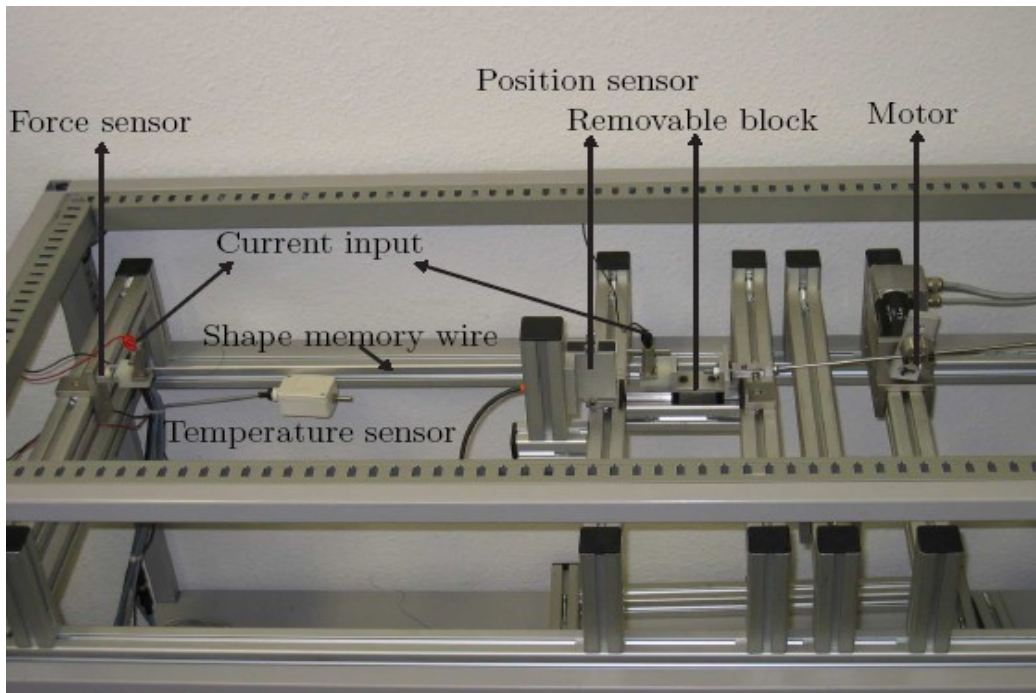


Figure 2.2. The SMA Test Rig

2.3. dSPACE System

The dSPACE system is a real time data acquisition system that is needed to interface system parts, to close the loop, and to modify and calculate the control algorithm in real time. The dSPACE is responsible for converting the analog signals from the sensors of the test rig plant into digital electrical signals via Analog to Digital Converters (ADCs) and processing the data via Digital Signal Processors (DSPs) to generate the data that can be manipulated by the computer through the dSPACE control software graphical user interface, called dSPACE ControlDesk. Any changes in the control or process variables through this interface will be manipulated in the plant in real time by converting these digital signals into analog signals via Digital to Analog Converters (DACs) that the plant can deal with, closing the loop that contains the hardware and software components.

The dSPACE with its hardware DS1104 DSP board connected via an Industry Standard Architecture (ISA) slot to the computer and interfacing the connection to the SMA test rig via the CP1104/CLP1104 connector panel. And with its ControlDesk software

directly interfaced with MATLAB/SIMULINK. Appendix A.1 shows a snapshot of the user interface of the dSPACE ControlDesk.

The dSPACE high performance digital control system used in the experiments is release 3.4, and dSPACE references are used to build and run experiments, to map the connections to the SMA test rig sensors in the SIMULINK Input/Output (I/O) signal's blocks, and to define the connections of the DAC/ADC for dSPACE to their corresponding locations in the Real Time Interface (RTI) blocks in SIMULINK or called input to controller and output of controller blocks [14, 15].

2.4. MATLAB/SIMULINK

MATLAB/SIMULINK is a programming/modeling and simulating tool used to write algorithms and to analyze dynamic systems. Coupled with Real Time Workshop (RTW), the SIMULINK block diagrams with the dSPACE embedded RTI blocks used in designing the controller or the model of the SMA wire which can be built and converted into real time C code, compiled and downloaded to the DS1104 DSP board. Then experiments initiated and run in the dSPACE ControlDesk software that controls the DSP and allow making experiments, then testing changes and monitoring variables of the controller, process, and plant in real time. The MATLAB/SIMULINK version 6.1/5.0 used to write the algorithm for the wire temperature calculations solving the heat transfer equation, to read data files from the experiments, and to build different control models.

2.5. Experimental preparation

Experimental preparation includes all the steps needed to make the overall system components interacts and communicates in the right order. Figure 2.3 shows an abstract block diagram illustrating the flow of signals in different parts of the experimental setup. The flow of the analog signals from the SMA wire and the sensors to the dSPACE, and the flow of the converted digital signals from dSPACE back to the SMA wire.

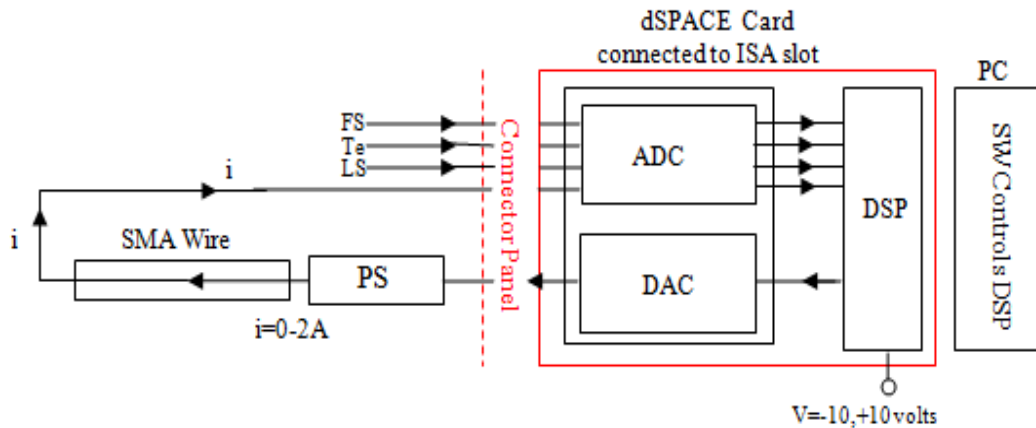


Figure 2.3. Flow of signals in the experimental setup.

The main blocks for building and running experiments were prepared; the dSPACE connector panel ports and their corresponding links interfacing the SMA test rig data to the SIMULINK RTI environment are shown in appendix B.1 to B.6.

2.5.1. Testing the Hysteresis

The first set of the experiments were to test the hysteretic behavior of the SMA explained in section 1.3 under different criteria's. This includes testing the effect of changing constant load, motor variable load, frequency of the input signal, and different amplitudes of the input signal on the hysteretic behavior of the SMA material, similar to the work of Quing [13]. To see the hysteretic behavior an approximation is done using the MATLAB code in appendix A to calculate the wire temperature using runge-kutta 4th order numerical method via reading from the data files stored after each experiment in dSPACE. This intermediate level help in understanding the material behavior and in one of the research objectives to build a model through testing it in a feedforward controller. Figure C.2 and C.3, appendix C show the hysteretic behavior of the SMA, and other signals from sensors in the SMA test rig.

A general conclusion according to observations on the hysteresis behavior was that the SMA hysteretic behavior is affected by frequency, amplitude of the current input signal, and the load attached to the SMA wire:

1. At frequencies higher than 0.1 Hz, the frequency signal can be considered as a direct current (dc) signal with no changes so that the SMA does not exhibit hysteresis or shape memory effect i.e. positive or negative elongation is exhibited at high frequencies.
2. At frequencies lower than 0.1 Hz the material recognizes the change in the input and reacts accordingly.
3. No major differences are observed experimentally from different amplitudes of the input current. So, the material hysteretic reaction to sinusoids with 1A, 2A, and 3A amplitudes were exactly the same according to hysteresis plots based on approximations of the wire temperature.
4. No input currents higher than 2A are allowed since high current make a shear force that cuts the wire into two pieces.
5. Using different constant loads of 0.5 kg, 1 kg, 2 kg, 3 kg, and 4 kg have no major effect on the SMA hysteresis.
6. A very high constant load or a manual high tension on the SMA wire is capable of causing a functional fatigue in the material. The material has a lifetime based on the actuation cycles it responds to and it's around 50 hysteresis cycles for the NiTi SMA wire used in the experiments. So, the SMA wire is changed so many times during the experiments.

Other experimental observations while testing the hysteretic behavior of the SMA are also used to deduct a dynamic model of the SMA wire. However, part of the system dynamics is unknown which is the friction in the mass pulley and in the slider surface that has a non negligible effect to the measured force. A general observation from the force sensor measurements was that the force input to the system varies between 17.5 to 30N. And the current associated to these input forces varies between 0 to 1.7A respectively. And this leads to a logical inference that under high current i.e. heating phase the tension force required for contraction of the SMA wire in the austenite phase, to cancel friction, and to pull the mass up must be higher than the force in the case of zero current i.e. cooling phase for expansion of the SMA wire in the martensite phase

pushing the mass down. The constant mass used forms a variable load during runtime. Note that all experiments afterwards were done without the existence of the variable load from the motor, since it was disconnected from the test rig.

Chapter 3

Model- and Behavioral-Based Control of SMA

3.1. Introduction

The purpose of the model- and behavioral-based control of the shape memory alloy wire is to build a robust predictive model that can lead to a robust control of this nonlinear material. The nonlinear material doesn't only change the behavior according to the excitation signal but it changes its characteristic parameters during the lifetime of the input change. Therefore, this type of behavior encourages the adoption of this approach and experimenting its results. The model-based control approach is used to build a controller based on a known mathematical model of a characteristic parameter of the actuator plant, which can control the SMA wire behavior according to the model. This model-based approach for controlling the SMA is used in the O-Model feedforward controller which will be discussed in section 3.4. However, behavioral-based control of the SMA is used to build a controller model according to the behavior of the SMA wire under different conditions of heating and cooling where it behaves in different manners identified by the two phase transformations; the austenite and the martensite. Here, the plant dynamics will not respond to parametric changes in the model but it will change according to the expected behavior. This behavioral-based control approach for controlling the SMA wire is used to build two controllers the AM-Model and the V-Model feedforward controllers which will be discussed in section 3.2. Two different intersecting approaches are examined here, and both cannot be validated due to different reasons that will be mentioned in section 3.3.

3.2. Behavioral-Based Approach

Behavioral-based controllers designed here are based on using the heat transfer equation to find the desired elongation of the SMA wire according to the temperature changes assigned with input current changes. This elongation is feed into a PI controller which will then output the current needed for the plant to enforce the SMA wire to move i.e. either to contract or to expand to the required position. Figure 3.1 shows the schematic diagram of the behavioral-based controller approach. The input to the heat transfer function block is the SMA wire current (i) to find the temperature (T) of the wire, then this wire temperature is the input for the model built according to

different criterias to find the desired elongation i.e. the expansion or contraction, then the PI controller measures the current needed for the SMA wire to move the SMA wire from its actual position (L_a) to the desired position (L_d), and this process applies to each manual change of the input current from the power supply.

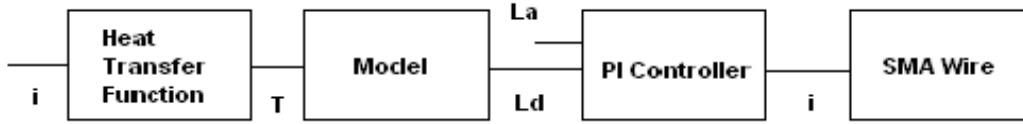


Figure 3.1. Schematic Diagram of the Behavioral-Based Feedforward Controller Main Blocks.

3.2.1. The AM- Model

The AM Model is a model of Austinite-Martensite phase transformations of the SMA. The idea was to use the heat transfer function and to move it from an estimate of the heat transfer in the SMA material as a normal conductor, to an equation that includes the behavior of the SMA wire. Relating both the heat transfer affected by changes in current and temperature of the wire with the change in the length of the SMA wire. And this can only be achieved by using the equation of the electrical resistance in terms of the length of the material.

Heating Phase- Austinite .3.2.1.1

The heat transfer thermal distribution equation is used to model the heating phase of the SMA wire, defined by equation 3.1:

$$\rho c V \frac{dT}{dt} = i^2 R - h A (T - T_e). \quad (3.1)$$

where ρ denotes the density of the SMA wire, c is the specific heat, V is the volume of the SMA wire, i is the current through the SMA wire, R is the electrical resistance of the SMA wire, h is the heat convection coefficient, A is the cross sectional are of the SMA wire, T is the temperature of the SMA wire, and T_e is the temperature of the

environment surrounding the SMA wire. The heat dissipation due to radiation and conduction is neglected from the equation, while $i^2 R$ is the heat generated from the external power source. And $h(T - T_e)$ is the heat convection.

Equation 3.1 as is doesn't model any type of behavior for the SMA wire; so to relate it to the behavior of the SMA at the heating process, or called going to the austinite phase; an understanding of system input that causes a certain behavior is needed; applying a variable current (i) generates then the output response as a change in the length of the SMA (L). Hence, increasing the temperature of the SMA when i is increasing.

The derived L for the heating part will be used to build a subsystem that converts a temperature input to the position of the SMA wire during heating. Therefore, the electrical resistance equation is used.

$$R = \delta \frac{L}{A}. \quad (3.2)$$

Where δ is the electrical resistivity of the wire, L is the wire length, and A is the cross sectional area of the wire. Substitute equation 3.2 in 3.1.

$$\rho c V \frac{dT}{dt} = i^2 \delta \frac{L}{A} - h A (T - T_e).$$

Then, the following equation defines a relation between the temperature and the elongation of the wire, where the elongation can be decided by subtracting the L value from the original length of the wire, according to the changed variables in the experiments.

$$L = \frac{\rho c V A \frac{dT}{dt}}{\delta i^2} + \frac{h A^2 (T - T_e)}{\delta i^2}. \quad (3.3)$$

Equation 3.3 forms the austinite Subsystem that is tested experimentally in a feedforward and PI controller. Note that this equation applies to the heating phase i.e. the austinite phase only. And it takes into consideration the change in the length of the wire accompanied with a change in the electrical resistance of the material, while it doesn't take into consideration other changes; like the change in the electrical resistivity of the wire, the heat convection coefficient, or the volume of the wire. However, for the martensite phase, it can exist under heating conditions just when an external stress force is applied that is capable to deform or to expand the SMA wire. So, it's not covered by this model.

Equation 3.4. shows another austinite model in terms of wire temperature as its input and a known L_d (desired position) and L_a (actual position) then the current as an output of the subsystem can be found according to the required elongation. This model is not tested experimentally.

$$i(t) = \sqrt{\frac{\rho c V \frac{dT}{dt}}{R} + \frac{hA(T - T_e)}{R}}$$

$$i(t) = \sqrt{\frac{\rho c V A \frac{dT}{dt}}{\delta L} + \frac{hA^2(T - T_e)}{\delta L}}. \quad (3.4)$$

Figure 3.2 shows the SIMULINK controller model for the austinite phase that is tested in a feedforward controller. See appendix B7 to B9 for the masked blocks under the SIMULINK blocks used in this controller.

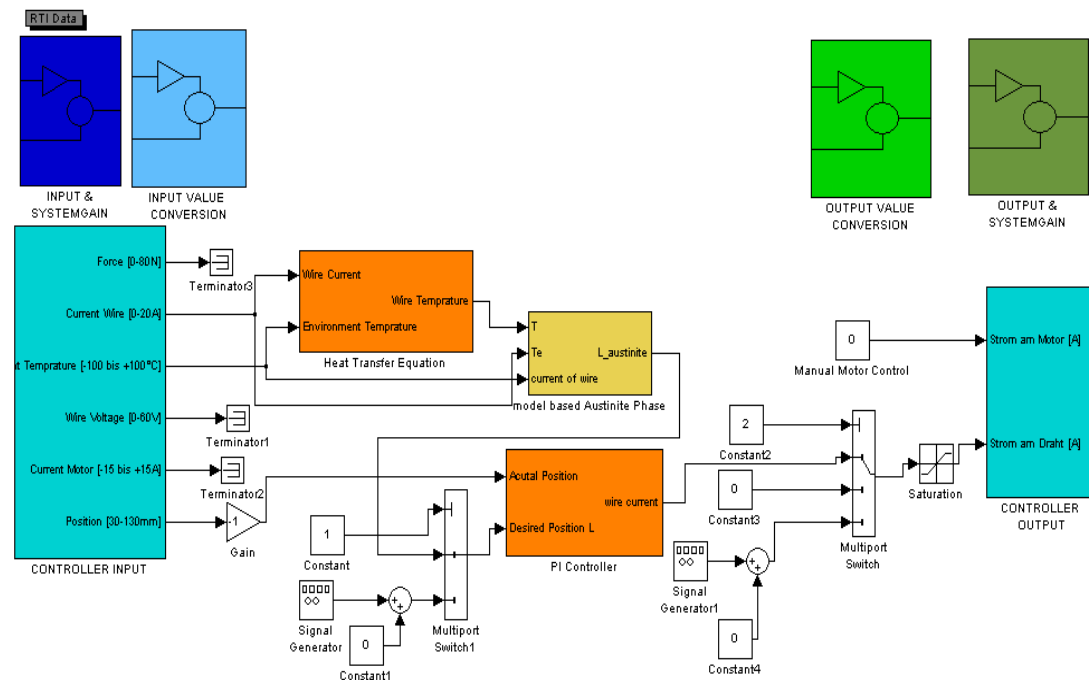


Figure 3.2. The Austinite Model Feedforward and PI Controller

Cooling Phase- Martensite .3.2.1.2

An assumption that the material changes from a passive element to an active element was made to model the behavior of the SMA wire under the cooling phase. The behavior of an SMA is mostly resistive and at cooling it acts like a capacitor, so the elongation of the material surfaces from their cubic case at austinite to the deformed shape at martensite releases an energy similar to a stored electrical capacitive energy, and this released energy is shown as an expansion of the wire also in the movement of the connected mass, i.e. a case of energy conversion from electrical to mechanical.

The reason behind this idea or assumption of energy conversion is that the existing mathematical models of the SMA parameters don't consider the non-resistive part of the SMA. A mathematical equation derived for an SMA spring which relates the electrical resistance with the applied strain and temperature [1], while no studies are done to show if there is any non-resistive components in the SMA. However, another mathematical equation derived for the SMA spring that defines the material state by a fraction called the martensite fraction which relates the deflection and temperature of the SMA material [16]. The full transformation of an SMA to martensite occurs at a

martensite fraction (η) of 0.8 to 0.9 and this fraction will be used in the assumption of a capacitive component later on.

To move from austenite to martensite at natural cooling i.e. $i=0$, the heat transfer equation cannot be used as is to calculate the elongation of the SMA since the $i^2 R$ is neglected here. Then, the assumption will be that capacitive energy E_c equals kinetic energy E_k experienced under cooling condition as follows:

$$E_c = \frac{1}{2} C V^2(t).$$

Where C: capacitance, and v (t): voltage.

$$E_k = \frac{1}{2} m v^2(t).$$

Where m: mass of connected load, and v (t): velocity.

Then the result for this assumption will be:

$$\frac{1}{2} C V^2(t) = \frac{1}{2} m v^2(t). \quad (3.5)$$

Approximate C to be the value of the martensite fraction $0.8 < \eta < 0.9$ to have full martensite phase transformation. And substitute the voltage in (3.5) in terms of ohm's law:

$$V(t) = R i(t).$$

And the velocity as the differentiation of the displacement of the mass in the y-direction which is equal to the elongation of the SMA in the x-direction:

$$v(t) = \frac{dL}{dt}.$$

This results in equation (3.6) that relates the length of the SMA material with the inputs to the system.

$$\eta R^2 i^2(t) = m \left(\frac{dL}{dt} \right)^2. \quad (3.6)$$

However, substituting equation (3.2) in (3.6) as follows:

$$i^2(t) = \frac{m}{\eta} \frac{A^2}{\delta^2 L^2} \left(\frac{dL}{dt} \right)^2.$$

Then, a model similar to the current austinite model in equation (3.4) can be derived for the martensite phase that is also not tested experimentally. But here $i=0$, since it's a natural cooling process, but the assumption will be kept as is for deriving the martensite model in terms of the wire length change as a function of temperature change in later stage.

$$i(t) = \sqrt{\frac{m}{\eta} \frac{A}{\delta L} \frac{dL}{dt}}. \quad (3.7)$$

Similar to steps done in modeling the heating part, a model that relates the position L for the martensite phase with the input temperature will be derived in order to control the position or shape memory behavior of the SMA under cooling. But note that under the same current but with certain amount of stress force, the wire can move into martensite phase even without cooling. In this case equalizing equation (3.4) and (3.7) will lead to the following:

$$L(t) = \int_{t_0}^{t_m} \left(\sqrt{\frac{\eta \delta L_a}{m A} \left(\rho c V \frac{dT}{dt} + h A (T - T_e) \right)} \right) \cdot dt. \quad (3.8)$$

Equation (3.8) relates L for the martensite phase with the temperature change, which is decreasing in this phase, L_a denotes the length of the SMA wire reached at austinite phase before cooling starts at time t_0 till the maximum expansion of the wire is reached at time t_m .

Figure 3.3 shows the SIMULINK controller model for the martensite phase that is tested in a feedforward controller.

See appendix B7, B8, and B10 for the masked blocks under the SIMULINK blocks used in this controller.

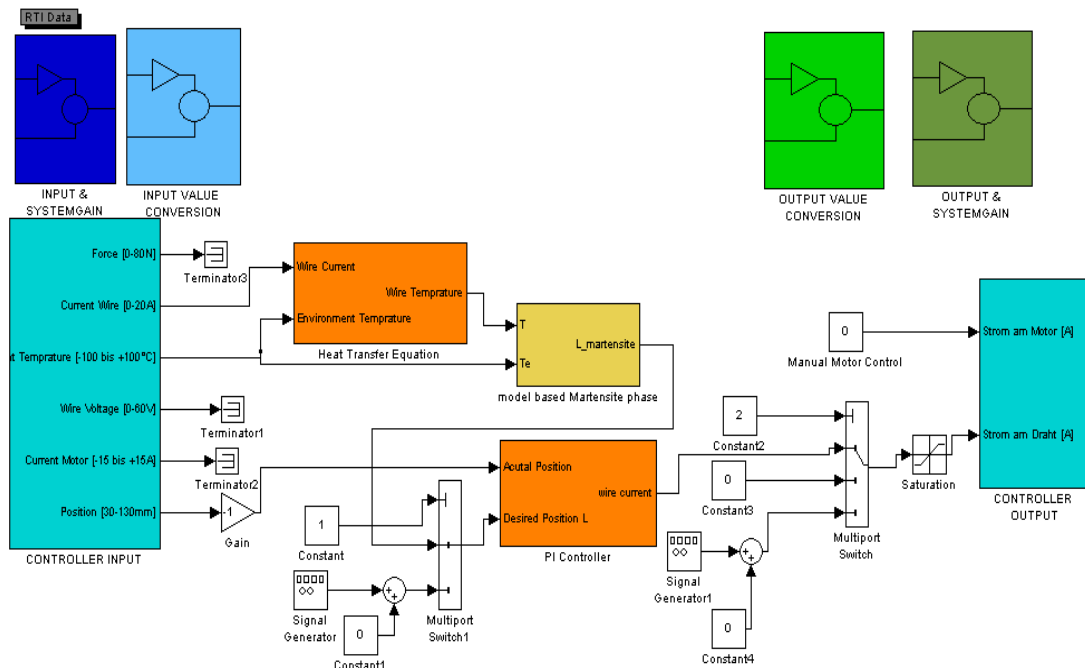


Figure 3.3. The Martensite Model Feedforward and PI Controller

Heating Cooling Combined .3.2.1.3

The heating cooling combined controller forms the AM-model. Both the austenite and martensite will be tested to see if the overall behavior of the SMA can be controlled in both sides of the memory effect or hysteresis.

Then equations (3.3) and (3.8) will be used. The selection criteria will be done through an if statement block and an if statement activated subsystems. The if statement block considers two conditions to make one of the subsystems active at a time, using a common write variable, memory, and read variable blocks:

$$i > 0 \quad \text{or} \quad \frac{dT}{dt} > 0 \quad \Rightarrow \quad L_{austenite}$$

$$i = 0 \quad \text{or} \quad \frac{dT}{dt} \leq 0 \quad \Rightarrow \quad L_{martensite}$$

Figure 3.4 shows the SIMULINK AM-model controller for the austenite-martensite phases of the SMA that is tested in a feedforward controller.

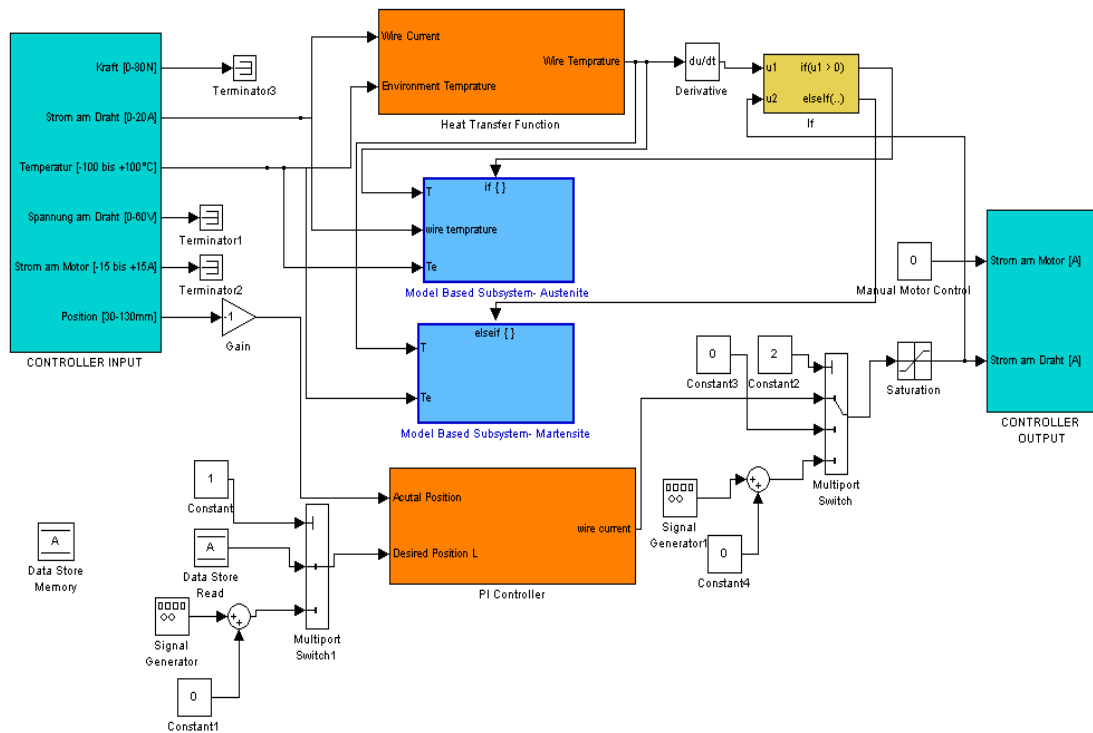
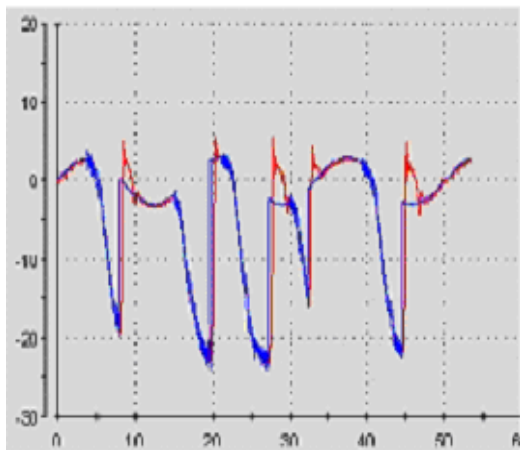


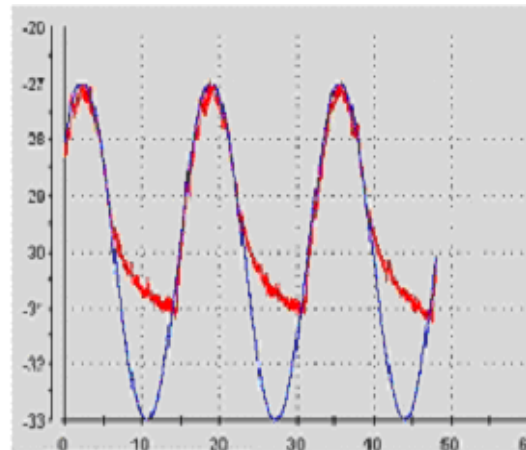
Figure 3.4. The AM Model Feedforward and PI Controller

Experimental Results .3.2.1.4

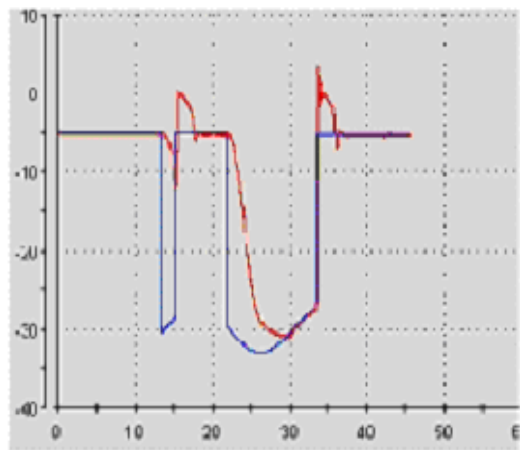
The set of controller models are tested in a feedforward control structure. The response from the models aren't perfect but they show follow-up of the actual position signal to the desired position signal. Figure 3.5 shows the set of results for the different models. The results of testing both models, the austenite and the martensite separately shows promising results. The output in the austenite case using a signal generator as an input switched to the model output and feed into the PI controller defines an arbitrary signal that the SMA material can follow, but it needs more validation; taking into consideration all temperature dependant changes in the behavioral heat transfer equation. However, the martensite model results shows a valid assumption of non-passivity in the material.



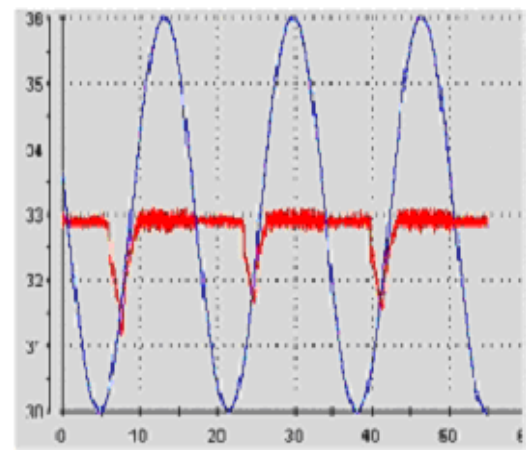
3.5.1. Austinite Model with signal generator as input



3.5.2. Martensite Model with signal generator input and Laustinite as input



3.5.3. Martensite Model with Lactual as input



3.5.4. AM-Model with signal generator as input

Figure 3.5. Austinite, Martensite, and AM models results in feedforward with PI controllers. Time in (s) versus actual position (red) and desired position (blue) in (mm).

3.2.2. The V-Model

The V-Model is an extension of the AM-model discussed previously. Here the idea is to take the volume change of the SMA into consideration in the heat transfer equation for calculating the desired length of the SMA wire.

Therefore, the volume change is expressed in terms of the length of the wire as follows:

$$V = AL. \quad (3.9)$$

Differentiate equation (3.9) by dL to get:

$$\frac{dV}{dL} = A. \quad (3.10)$$

Substitute equation (3.2) in equation (3.1):

$$\rho c V \frac{dT}{dt} = i^2 \delta \frac{L}{A} - hA(T - T_e). \quad (3.11)$$

Substitute equation (3.9) in equation (3.11) to get:

$$\rho c A L \frac{dT}{dt} = i^2 \delta \frac{L}{A} - hA(T - T_e).$$

Equation 3.12 forms the V-model mathematical formula that relates the change of the length of the SMA wire to the wire temperature change taking the volume change of the material into consideration, this system can be used to model the heating and cooling of the SMA wire neglecting the case when austenite moves to martensite under stress.

$$L = \frac{hA^2(T - T_e)}{\delta (i^2 - \rho c A^2 \frac{1}{\delta} \frac{dT}{dt})}. \quad (3.12)$$

Another derivation for the current of the SMA material, which is not tested experimentally:

$$i^2(t) = \rho c A^2 \frac{1}{\delta} \frac{dT}{dt} + hA^2(T - T_e) \frac{1}{\delta} \frac{1}{L}. \quad (3.13)$$

On the other hand, assuming heat distribution in all parts of the SMA wire i.e.

$dT / dL = 0$; then differentiation of equation (3.11) by dL leads to the following:

$$\rho c \frac{dV}{dL} \frac{dT}{dt} = \frac{i^2 \delta}{A}.$$

Substitute equation (3.10), a simplified relation between the temperature and the current can also be derived, and this is also not tested experimentally:

$$i^2(t) = \rho c A^2 \frac{dT}{\delta dt}.$$

$$i(t) = \sqrt{\rho c A^2 \frac{dT}{\delta dt}}. \quad (3.14)$$

Figure 3.6 shows the SIMULINK controller model for the V-model that is tested in a feedforward controller. See appendix B11 for the masked blocks under the SIMULINK blocks used in this controller.

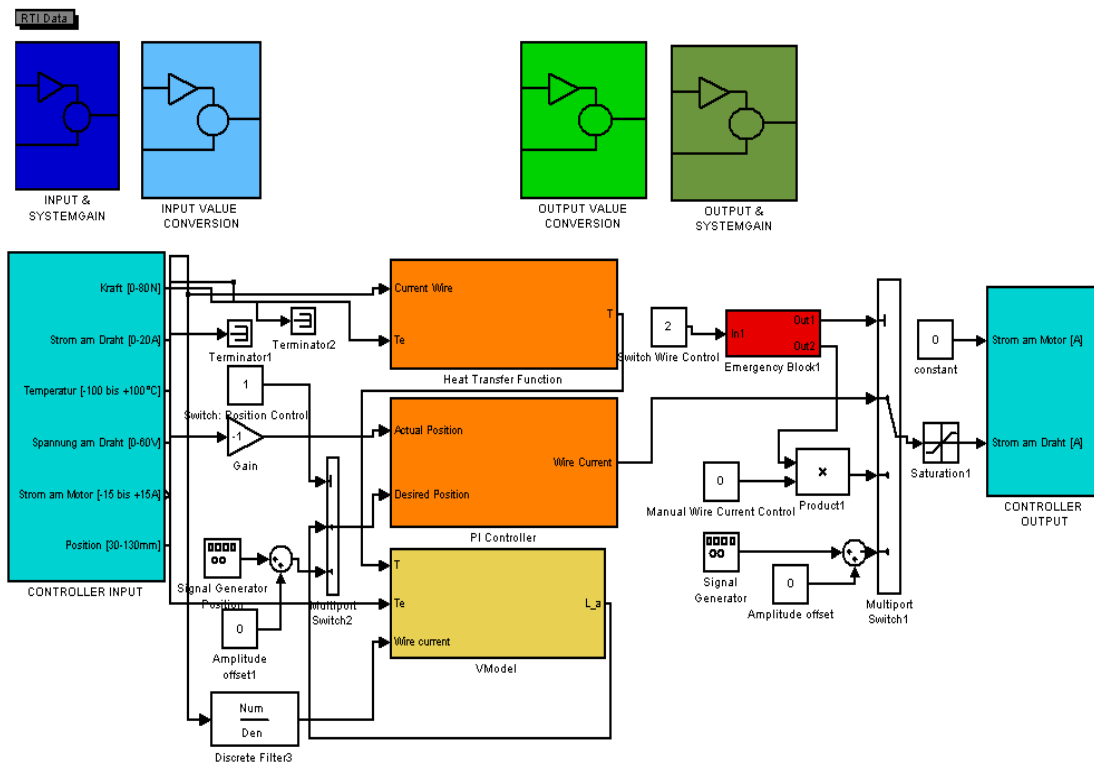


Figure 3.6. The V-Model Feedforward and PI Controller

Experimental Results .3.2.2.1

The V-model is tested and was unable to control the position of the SMA. Figure 3.7 shows the results of using the V-model in a feedforward with a PI controller. To let the controller respond, the signal generator input was used as the input desired position

instead of using the desired position from the output of the V-model subsystem directly. The response is from the PI controller not from the model due to the mismatch between the real temperature and the calculated wire temperature.

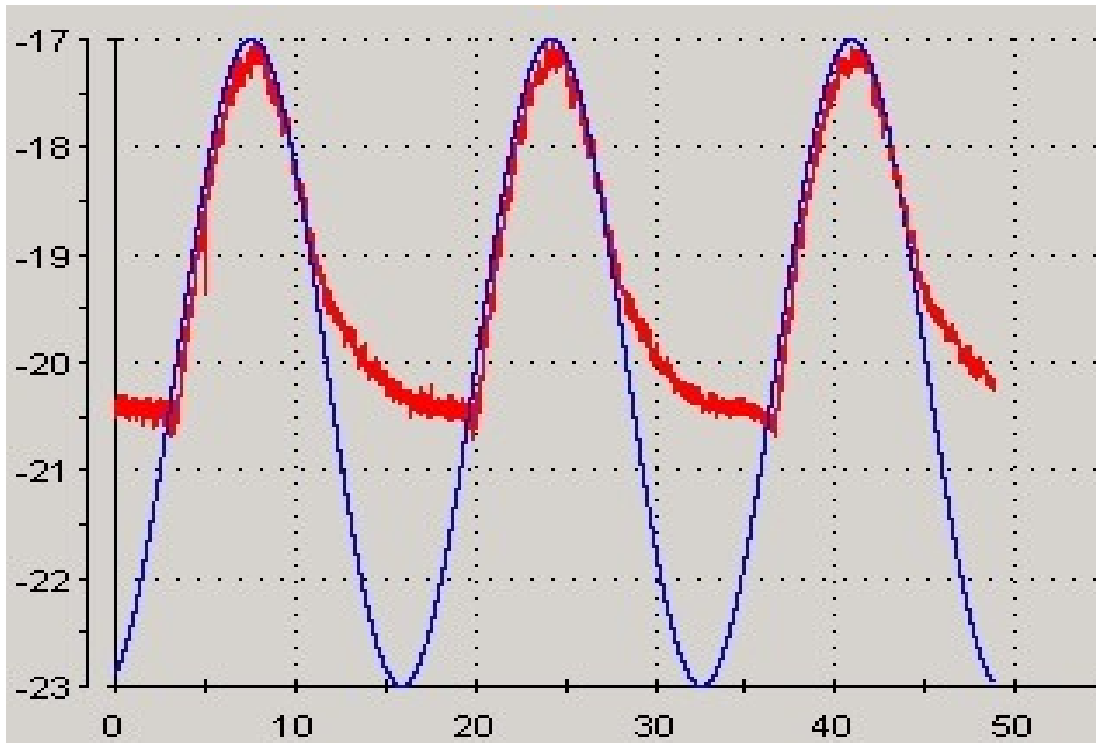


Figure 3.7. V-Model results in feedforward with PI controllers. This is using the signal generator as input. Time in (s) versus actual position (red) and desired position (blue) in (mm).

3.3. Conclusions on the Behavioral-Based Approach

The conclusion of testing the behavioral-based models according to ideas and assumptions that takes into consideration behavioral aspects and changes in some parameters of the SMA wire to control its position. These ideas summed into two different behavioral models; the AM-model and the V-model were unable to control the position of the SMA wire due to different reasons:

1. There is no practical way that can measure the wire temperature. Hence, there is no online measurement of it since the wire temperature is not equal in the different points of its surface.
2. The heat transfer equation SIMULINK model that is used to approximate the wire temperature using numerical methods needs computation time that doesn't match the fast temperature changes of the SMA wire in real time, i.e. unlike the case of online sensor measurements. And since the models are all temperature dependant, while they include a derivative term of the temperature which will be zero at steady state the models cannot be validated.
3. The heat transfer function used as a basis to derive the elongation measurements in the SMA material is derived as a general case for heat equilibrium in metals, while in the case of the SMA, many variable parameters should be considered in solving this equation, the resistance, the length, the volume, the density, and the heat coefficients. That were not all considered in these models.

3.4. Model-Based Approach

The behavioral-based control derived in previous sections is a new approach in shape memory alloys to tackle the usage of the heat transfer equation as the behavioral model, to discuss a non-passivity of the material, and to consider the effect of volume change in the SMA material. While these behavioral approaches cannot be validated as mentioned previously, the next step will be to test the possibility of using a model-based controller using a model for the SMA from the literature, which is derived based on experiments on the SMA. There are no mathematical models found for the SMA except few that are more related to mathematical models of hysteresis or models on different multiple hysteresis in the material, which cannot be used in this research.

The model-based approaches depend on having a representative model of a process and using an inverse of the model of the system. In this research, a mathematical model for one of the changing parameters of the SMA wire will be used which is the electrical resistance. The change in the SMA electrical resistance as a function of temperature is

hysteretic. Then, the resistance model will be used to build the Ohm-Model to serve the purpose of position control of the SMA.

3.4.1. The O-Model

The O-model is the abbreviation of Ohm-model. The idea here is to use Ohm's Law to calculate the current needed to feed the SMA under the accompanied changes of the SMA resistance during different heating and cooling cycles. The resistance mathematical model in equation (3.15) is derived in a study for R. Velazquez et al. [1] depending on an empirical relation proposed by Liag and Rogers [16] which gives the martensite fraction in terms of temperature.

The model is a resistance model for an SMA spring in terms of temperature and deflection i.e. elongation of the material. Although, the experiments used an SMA wire and not an SMA spring, but the wire itself behaves similar to a spring with unknown stiffness [9], so the same formulas can be used for the SMA wire as an assumption without problems.

$$R_a(\delta, T) = \begin{cases} 2.97 + 0.5e^{0.13\delta} & , \quad T \geq A_s \\ 1.97 + 0.5 e^{0.13\delta} + \cos\left(1 + \frac{\delta}{L}\right)\left(\frac{T - A_s}{A_f - A_s}\right) & , \quad A_s \leq T \leq A_f \\ 0.87(2.97 + 0.5 e^{0.13}) & , \quad T \geq A_f \end{cases} \quad (3.15)$$

Equation (3.15) defines the resistance of the SMA as function of δ the deflection or elongation and T the temperature of the SMA wire. The resistance changes according to the start and final temperatures of the austinite phase.

Then, to have a complete mathematical resistance model for the SMA to use it for modeling the behavior in both directions i.e. heating and cooling, the resistance function for the martensite phase will be derived as well. And since the austinite has less resistance than the martensite, while martensite phase starts with the resistance of the final austinite phase, reversing the temperatures and the equations order will be

done to develop the mathematical model of the martensite resistance as follows in equation (3.16):

$$R_m(\delta, T) = \begin{cases} 0.87(2.97 + 0.5 e^{0.13}) & , \quad T \leq M_s \\ 1.97 + 0.5 e^{0.13\delta} + \cos\left(1 + \frac{\delta}{L}\right) \left(\frac{T - M_s}{M_f - M_s}\right) & , \quad M_s \leq T \leq M_f \\ 2.97 + 0.5 e^{0.13\delta} & , \quad T \geq M_f \end{cases} \quad (3.16)$$

Equation (3.15) will be the active subsystem when heating the SMA and equation (3.16) will be the active subsystem when cooling the SMA.

Using Ohm's Law:

$$V = IR.$$

Where V is the voltage, I is the current, and R is the resistance. The input voltage to the system is used to measure the change in the current of the SMA according to the resistance changes when temperature is changed. The phase transformation temperatures used to build the O-model can be found in table C.3, appendix C. These values are taken from the experimental results of Kötter [12] on the same SMA wire used in the experiments.

Figure 3.8 shows the SIMULINK controller model for the O-model that is tested in a feedforward controller without PID usage. See appendix B12 and B13 for the masked blocks under the SIMULINK blocks used in this controller. The if statements selection criteria was explained previously is the phase transformation temperatures.

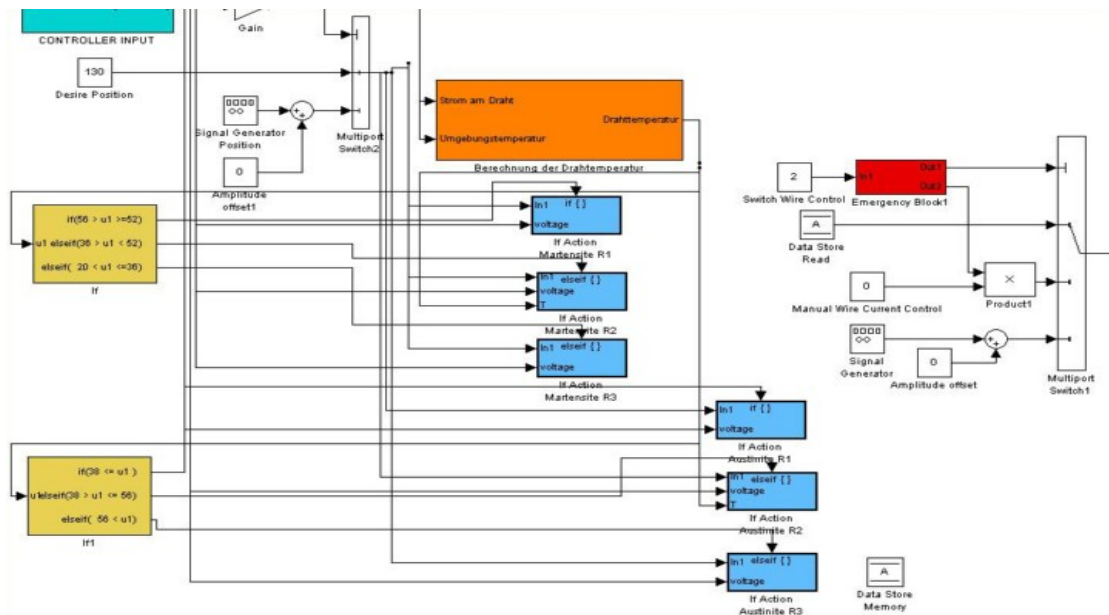


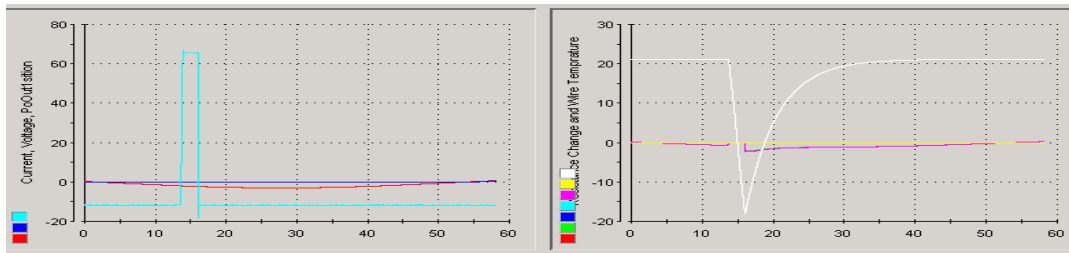
Figure 3.8. The O-Model Feedforward Controller.

3.4.1.1. Experimental Results

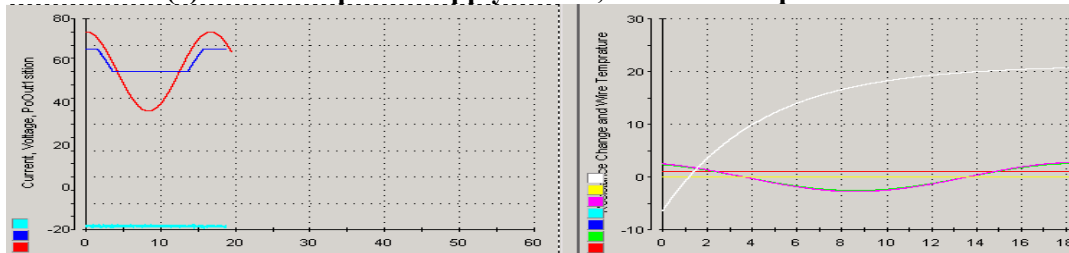
The Ohm model-based controller was unable to control the position of the SMA. The reason is also that the model cannot be validated since its dependant in the change of the wire temperature that cannot be measured by a temperature sensor as it's not equal in all points of the SMA material surface, and computations of the temperature using the heat transfer equation don't match the real time requirements of the system.

Figure 3.9 shows how the problem in the calculation of temperature of the wire is the reason for the non response of the controllers tested. The response in extreme inputs i.e. switch on or switch off cases of the power supply based on the natural dynamic behavior of the SMA wire, so it's not based on the calculated temperature of the wire.

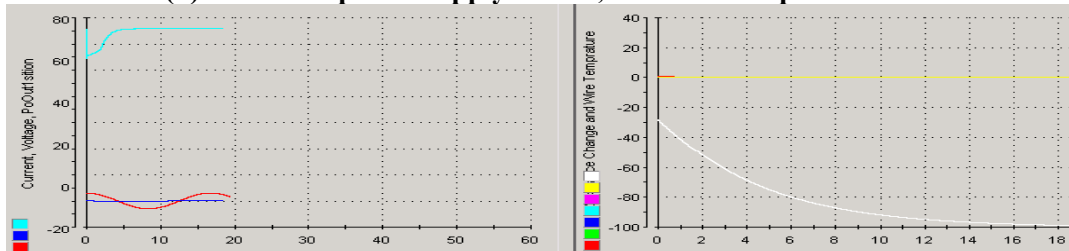
A fast manual switch on of the power supply in (a) and (b) doesn't show the real T_{wire} reached. A fast switch off of the power supply in (c) shows a fast decay of T_{wire} but not to the real T_{wire} reached. The selection criteria for the expected resistance at a certain temperature of the wire is not working due to the problem in wire temperature calculations. So, the expected corresponding current is not the value required for the SMA wire to control its position.



(a) Switch on power supply results, no success in position control



(b) Switch on power supply results, no success in position control



(c) Switch off power supply results, no success in position control.

Figure 3.9. O-Model results working as a feedforward controller. The curves to the right show the changes in resistance (colored). Wire temperature (white). The curves to the left show the current change according to manual voltage change and so the actual position in (cyan).

Conclusions on the Model-Based Approach .3.5

Model-based controller was unable to control the position of the SMA wire, due to its dependability on the temperature of the wire changes that cannot be measured.

The next step will be experimenting the non model-based approach and testing the possibility of using PID and PID adaptive controllers since there is a good response from the PI when signal generator input has been chosen in previous experiments, while generally PI controllers are used for actuator plants like in the SMA. However, an adaptive controller will also be a good choice since no plant dynamics can be derived as there are a lot of unknowns here, as it will be shown in Chapter 4.

Chapter 4

Non Model-Based Control of SMA

4.1. Introduction

Non model-based control includes different kinds of control types, some research have been conducted for the position control of SMAs using non model-based approaches; using current limiter and power limiter PID controllers, using fuzzy logic, or using neural network and sliding mode controller [17, 18, 19]. And since the aforementioned model-based and behavioral-based controllers cannot be validated due to the issue in following the wire temperature changes. Two different non-model-based approaches to control the position of the SMA will be derived and experimented here; the PID controller, and the PID adaptive controller.

4.2. PID Controller

Proportional Integral Derivative (PID) controller is the most widely used non model-based controller in the industry. Figure 4.1 shows the diagram of a PID controller. From the diagram it's easy to notice that proportional means the output is proportional to the error, integral means the output is proportional to the integral of the error, and derivative means the output is proportional to the derivative of the error, and each has a special gain denoted by proportional, integral, and derivative parameters which are k_p , k_i , and k_d respectively. Proportional block increases the sensitivity of the controller to system error. Integral block accelerates the speed of the controller to the required reference. And derivative block increases the control stability while slows the change in the controller output [20].

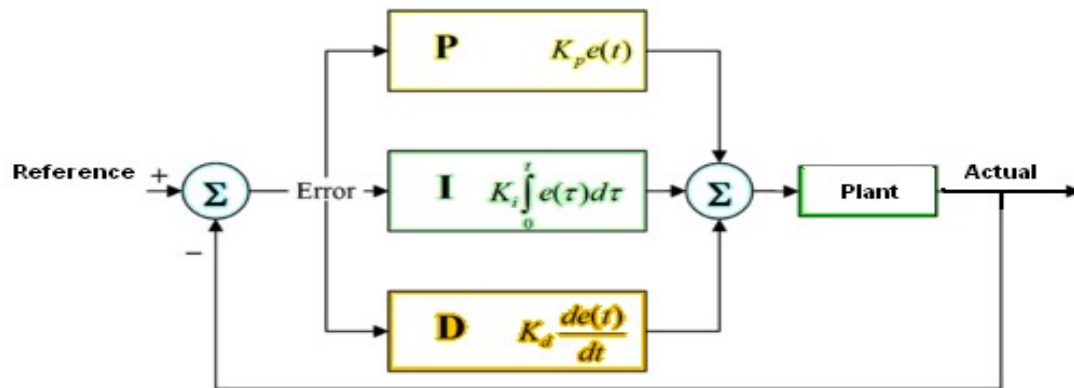


Figure 4.1. PID Controller.

4.2.1. PI Position Control Experimental results

The first experiments will be to use a PI controller trying to control the position of the SMA wire. There are special tuning algorithms for the PID like Ziegler Nichols [21] based on different criterias like step response of the plant or critical gain and critical period. But here, manual tuning is used optimizing the controller through the performance seen from experiments under different sets of K_p and K_i parameters. Figure 4.2 shows the SIMULINK of the PID controller used to control the position of the SMA. See appendix B8 for the masked blocks under the SIMULINK blocks used in this controller.

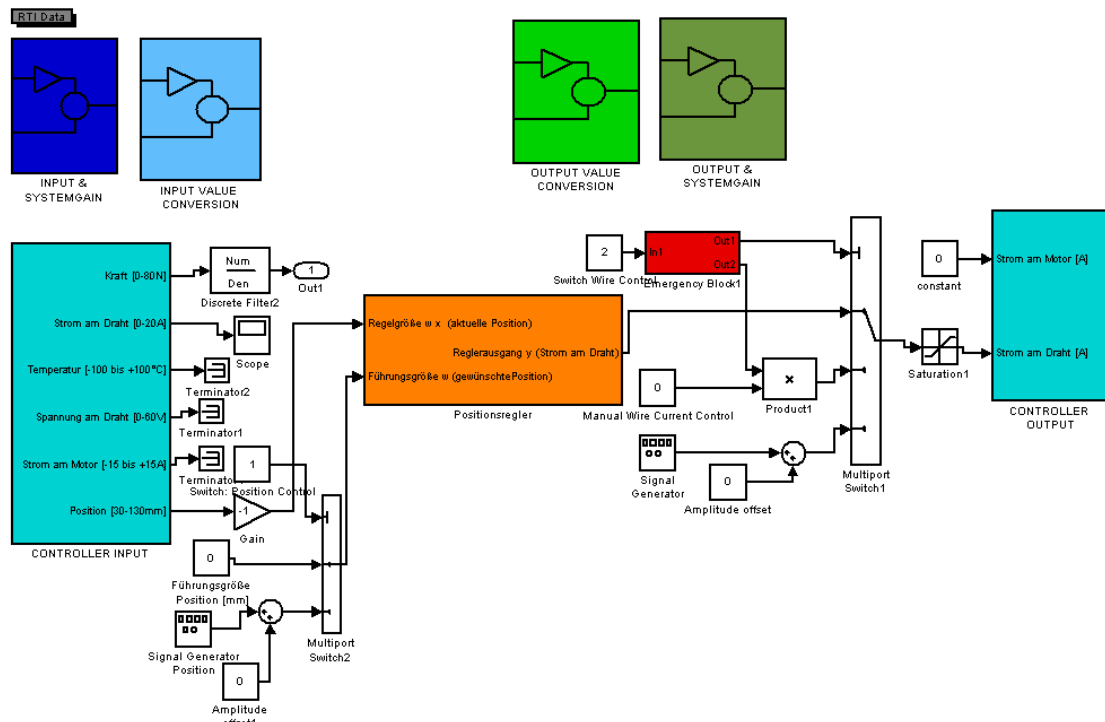
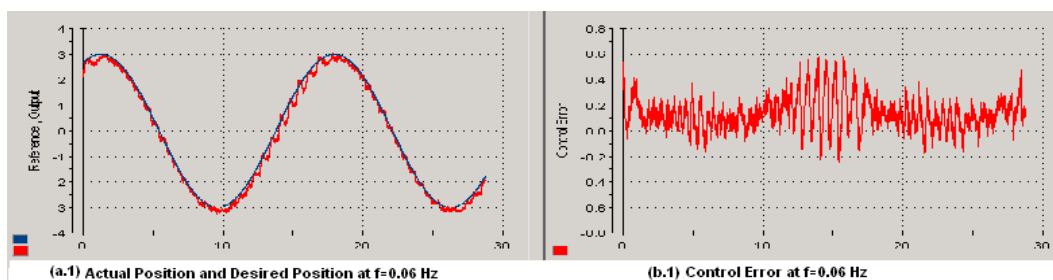


Figure 4.2. The PI Controller for position control of the SMA.

The results of the PI controller proves its ability to control the position of the SMA wire robustly with very small control error in the range of [0.1-1] mm. Under high frequencies in the input reference desired position above 0.1 Hz the control error increases since the SMA wire cannot follow the curve due to natural cooling delay due to heat convection, i.e. the SMA wire cannot follow such high frequencies of the desired position since the heating process is faster than the natural cooling process.

Figure 4.3. Shows the results of experimenting the PI controller under different set of frequencies. Note that the variable load through the motor is not part of the experiments, and the motor is totally disconnected from the test rig.



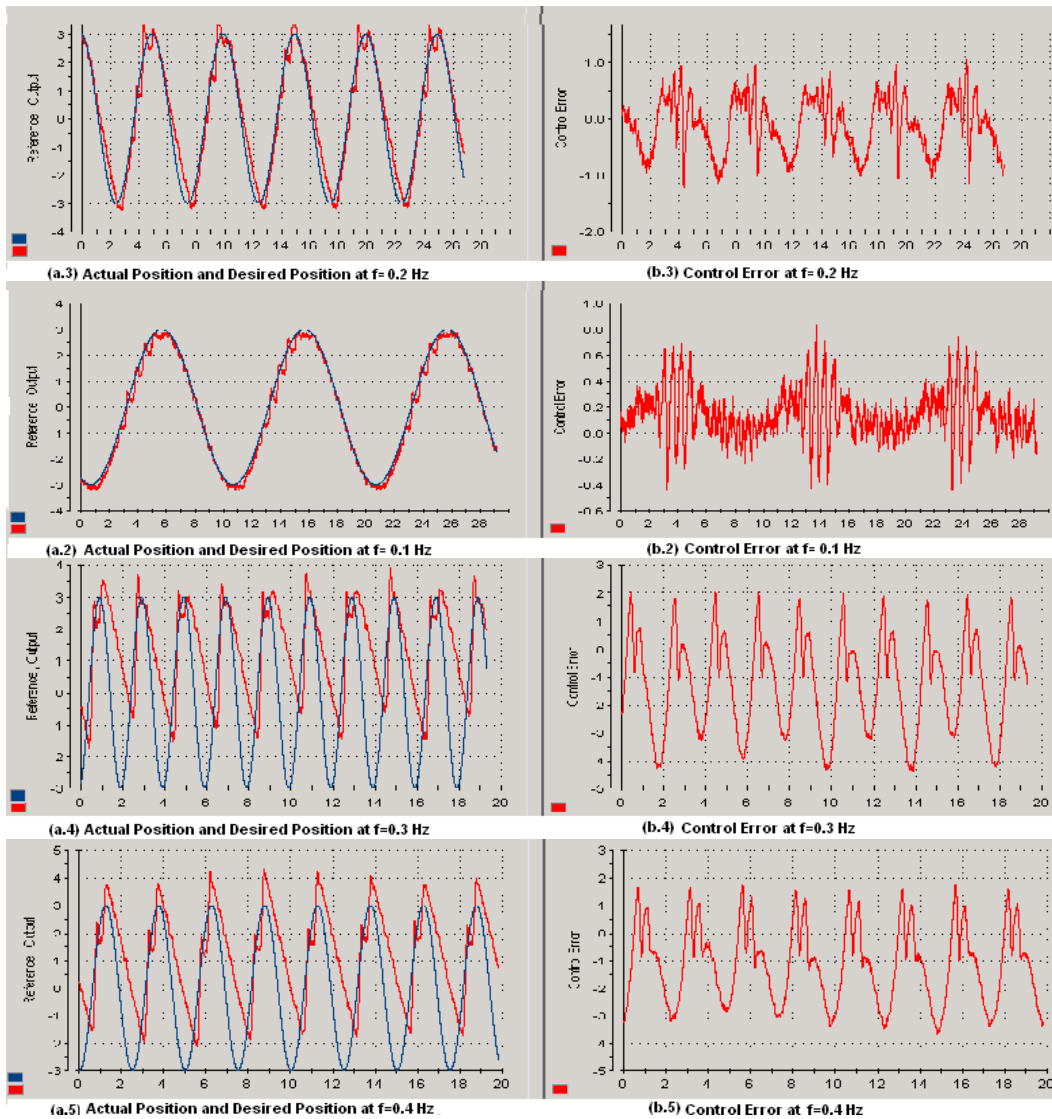


Figure 4.3. PI Position Controller Results, using $K_p=250$, and $K_i=20$. The desired input position is a sinusoid with amplitude=3. (a.1) to (a.5) Time in (s) versus actual position (red) and desired position (blue) in (mm). (b.1) to (b.5) Time in (s) versus control error under different frequencies of desired position.

Table C.4 appendix C lists the measured values for control error margin under different frequencies.

4.3. Adaptive Control

Since adaptive control performs a redesign of the controller in accordance to the changing parameters of the plant, adaptive control is a good choice in the SMA wire

plant case. The next sections will introduce the basic two approaches of adaptive control that leads to the way how the PID adaptive controller is derived and tested on the SMA wire.

4.3.1. MRAC Control

Model reference adaptive controller is shown in figure 4.4. The basic principle of this adaptive controller is to build a reference model that specifies the desired output of the controller, and then the adaptation law adjusts the unknown parameters of the plant so that the tracking error converges to zero [22].

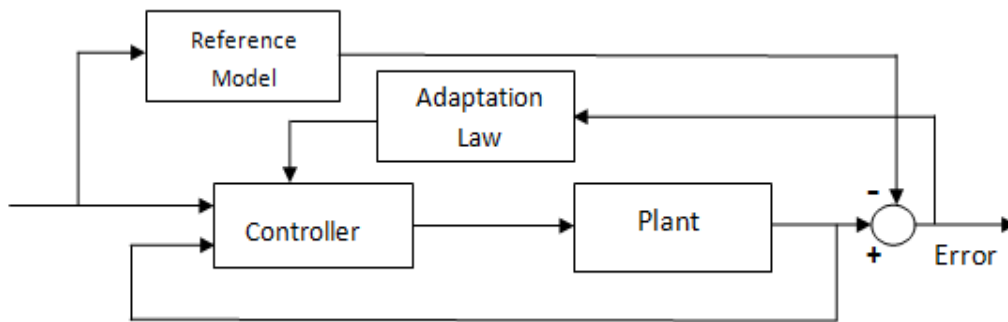


Figure 4.4. MRAC adaptive control system [22]

4.3.2. STC Control

Self tuning adaptive controller is shown in figure 4.5 [22]. The basic principle of this adaptive controller is to have a parameter estimator that estimates recursively the unknown parameters of the plant and feeds it to the controller. This recursive estimation based on the parameters that fits the past input-output criteria of the plant.

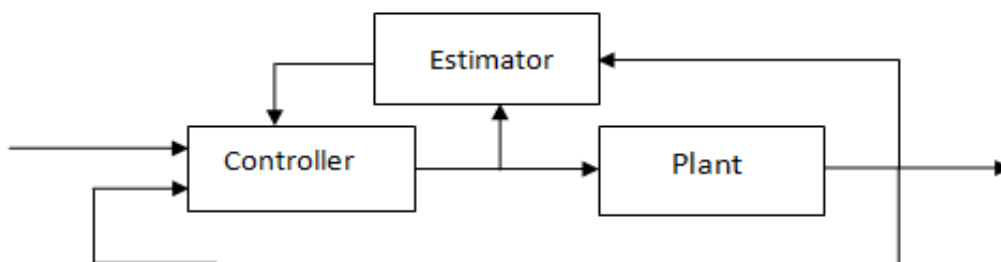


Figure 4.5. STC adaptive control system [22]

4.3.3. Designing the PID Adaptive Controller

For both MRAC and STC adaptive control approaches the plant dynamics cannot be estimated for the SMA. So, choosing an estimated parameter from the plant dynamics will not be an efficient way of handling the problem, testing the choice of position as an estimated parameter will be used in step1. A combined approach that joins MRAC and STC will be used for building a PID adaptive controller tested with very good performance. The reason for calling this approach a combined approach, since the estimated parameters will be the controller parameters that will adapt to the plant unknown parameters recursively like in STC, while the tuning will be according to the tracking error convergence to zero like in MRAC, since the reference model here is the plant itself as will be shown in step2.

Figure 4.6 shows the MRAC adaptive controller with a first degree plant and two estimated parameters [22].

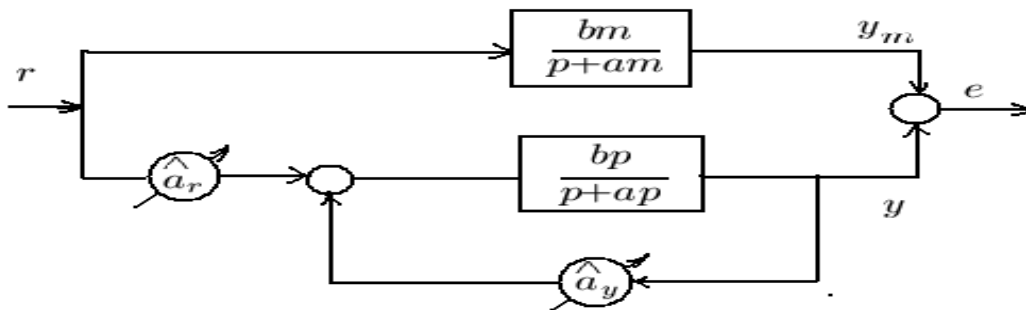


Figure 4.6. MRAC system for a first order plant [22]

The equations corresponding to the MRAC controller in figure 4.6 are the following:

$$v(t) = [r \quad y]^T. \quad (4.1)$$

Where $v(t)$ denotes the signal vector, r is the reference input signal, and y is the output signal.

$$\hat{a}(t) = \begin{bmatrix} \hat{a}_r \\ \hat{a}_y \end{bmatrix}. \quad (4.2)$$

Where $\hat{a}(t)$ is the vector of the controller adaptive parameters; defined by their derivatives in terms of plant parameters to derive the adaptation law as follows:

$$\begin{aligned} \hat{a}_r^{\bullet} &= -\text{sgn}(b_p) \gamma e r . \\ \hat{a}_y^{\bullet} &= -\text{sgn}(b_p) \gamma e y . \end{aligned} \quad (4.3)$$

Where, \hat{a}_r^{\bullet} is the derivative of the estimated parameter corresponding to the reference signal r and \hat{a}_y^{\bullet} is the derivative of the estimated parameter corresponding to plant output signal y , e is the error signal, $\text{sgn}(b_p)$ determines the direction of search for the proper controller parameter, and γ is the adaptation coefficient.

Step1: Building an adaptive controller

Choose position as the estimated parameter and the position error as the second estimated parameter.

Let the signal vector be:

$$v(t) = [e \quad y]^T.$$

Here e is the position error, and y is the actual position.

Let the controller estimated parameters be:

$$\hat{a}(t) = \begin{bmatrix} \hat{a}_e \\ \hat{a}_y \end{bmatrix}.$$

Where \hat{a}_e is the estimated parameter corresponding to error signal, and \hat{a}_y is the estimated parameter corresponding to actual position signal, then the adaptation law is the following:

$$\begin{aligned}\hat{a}_e^* &= -\text{sgn}(b_p) \gamma e^2. \\ \hat{a}_y^* &= -\text{sgn}(b_p) \gamma e y.\end{aligned}\tag{4.4}$$

Substitute b_p as 1 since there is no transfer function for the SMA wire dynamics to build the controller. Figure 4.7 shows the SIMULINK block diagram of the adaptive controller in (4.4). Note that The SIMULINK blocks and its interfaces used to build this controller are the same used in the PI control case. The only difference here is the masked block of the adaptive controller.

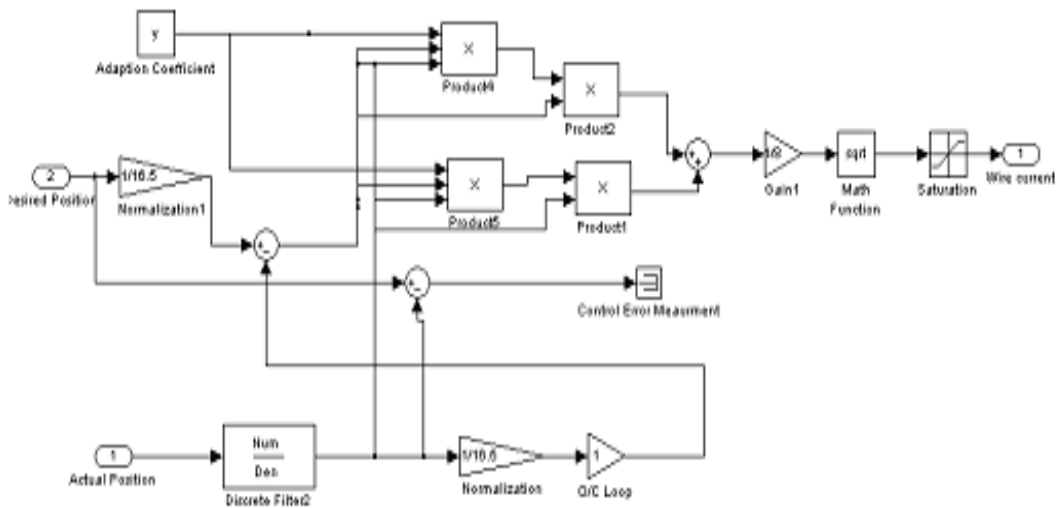


Figure 4.7. Adaptive controller based on adaptation law (4.4)

Step 2: Building the PID adaptive controller

In step 1, using the error signal as one of the signals used for adaptation helps the controller to react. And as there is no equation expressing the plant dynamics, to build a PID adaptive controller the assumption will be to use the controller parameters as the estimated parameters of the plant; while this will help the PID controller to self tune itself which is a combined approach of MRAC and STC. Figure 4.8 shows a block diagram describing the idea.

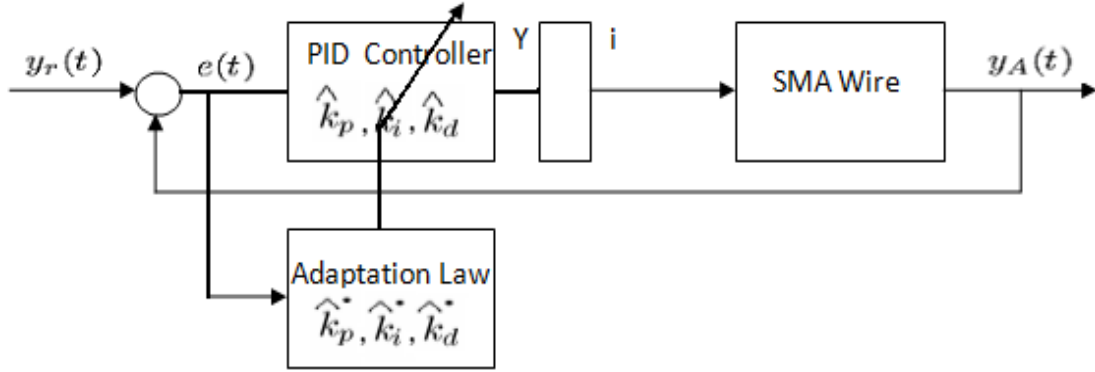


Figure 4.8. The PID adaptive controller combined MRAC and STC.

In figure 4.8, $e(t)$ denotes the error signal equals the desired position subtracted from the actual position of the SMA to insure convergence of the error to zero like in MRAC. The reference model of the MRAC is the plant itself; the adaptation coefficients are the estimator coefficients of the STC to let the PID adapt its controller coefficients to the plant. The block attached to the PID is a block to explain that the output of the controller is converted using blocks that derive the current into the SMA wire.

Based on the formulas of regular PID controllers, the idea in figure (4.8) that the \hat{k}_p^* , \hat{k}_i^* , and \hat{k}_d^* are the estimated parameters of the plant while they are recursively tuning their corresponding controller parameters as well with the following adaptation law, so that the PID controller coefficients are just the integral of the adaptation law.

$$\hat{k}_p^* = -\gamma e^2 \quad \Rightarrow \quad \hat{k}_p = \int -\gamma e^2 dt.$$

$$\hat{k}_i^* = -\gamma e \int e dt \quad \Rightarrow \quad \hat{k}_i = \int -\gamma e \int e dt dt. \quad (4.5)$$

$$\hat{k}_d^* = -\gamma e \frac{de}{dt} \quad \Rightarrow \quad \hat{k}_d = \int -\gamma e \frac{de}{dt} dt.$$

\hat{k}_p is the proportional gain, \hat{k}_i is the integral gain, \hat{k}_d is the derivative gain. While \hat{k}_p^* is the proportional estimated parameter, \hat{k}_i^* is the integral estimated parameter, and \hat{k}_d^* is the derivative estimated parameter. So the integral form of the estimated vector is:

$$\hat{a}(t) = \begin{bmatrix} \hat{k}_p \\ \hat{k}_i \\ \hat{k}_d \end{bmatrix}.$$

And the signal vector corresponding to each of them like normal PID controller signals as follows:

$$v(t) = \left[e(t) \quad \int e(t) dt \quad \frac{de(t)}{dt} \right]^T.$$

$$e(t) = y_A(t) - y_r(t).$$

Where $y_A(t)$ is the actual position of the SMA wire and $y_r(t)$ is the desired position.

The output of the PID Controller will be the following sum of the proportional, integral, and derivative outputs:

$$Y(t) = \sum_{P,I,D} \beta(i).$$

To simplify the representation of equations in time domain, the s-domain will be used. Where an integral is a division by s and a derivative is a multiplication by s. And instead of using t as the time samples, i as the iteration number will be used as follows:

$$\beta_P(i) = \gamma e^3(i) \frac{1}{s} = k_P e.$$

$$\beta_I(i) = \gamma e^3(i) \frac{1}{s^3} = k_I \frac{e}{s}.$$

$$\beta_D(i) = \gamma e^3(i) s = k_D e s.$$

Then the output of the controller can be expressed by the stable system shown below,

$$Y(i) = \sum_{P,I,D} \beta(i) = \beta_P(i) + \beta_I(i) + \beta_D(i).$$

$$Y(i) = \gamma e^3(i) \frac{(s^4 + s^2 + 1)}{s^3}.$$

To have the output current from the plant, these values of voltages should be divided by the resistance $R=8\Omega$ to approximate the current which is the square root of this value and saturated in the range 0 to 1.7 A as follows:

$$i(t) = \left\| \sqrt{\frac{Y(t)}{8}} \right\|_{\mathbf{0}}^{1.7}$$

Figure 4.9 shows the SIMULINK blocks for the PID adaptive controller in equation (4.5). A similar PID adaptive controller is derived by Feng Lin, et al. [23] using Frechet derivative and SISO system formulas, while here simplified formulas and combination of adaptive approaches lead to this model.

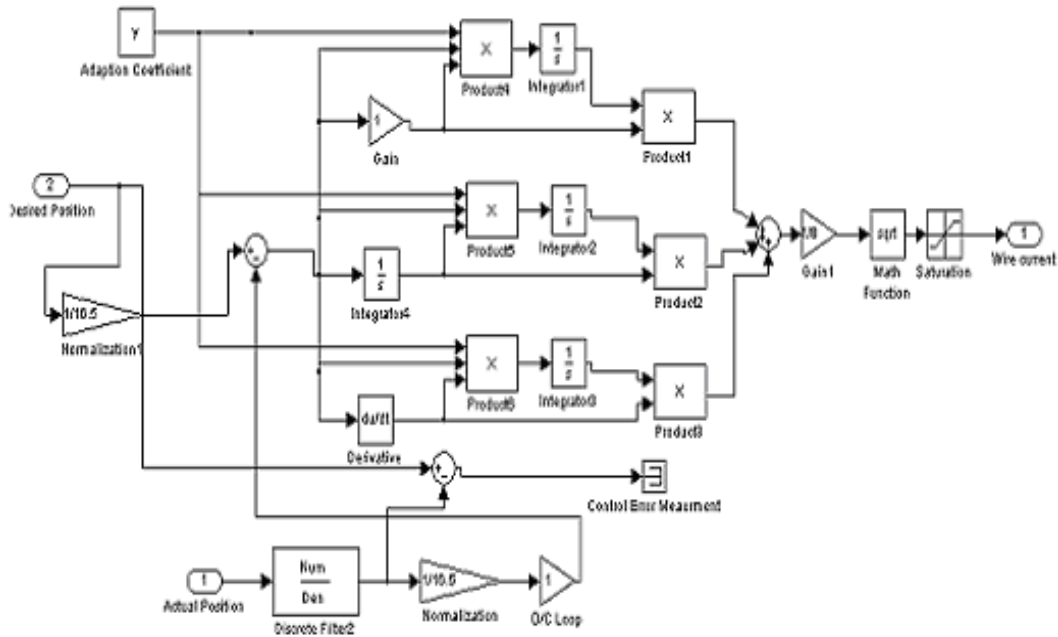


Figure 4.9. PID adaptive controller for position control of the SMA.

4.3.4. Experimental Results

Equations of MRAC controller with adaptation law (4.3) are tested experimentally and fail to have any response to control the position.

Refinement of equation (4.3) into (4.4) in *step1* to make the parameter dependant on the error signal instead of the reference signal makes the controller starts to work and control the position of the SMA, while the performance is low.

Figure 4.10 shows the results of testing the adaptive controller. The results show a possible position control but with high control error.

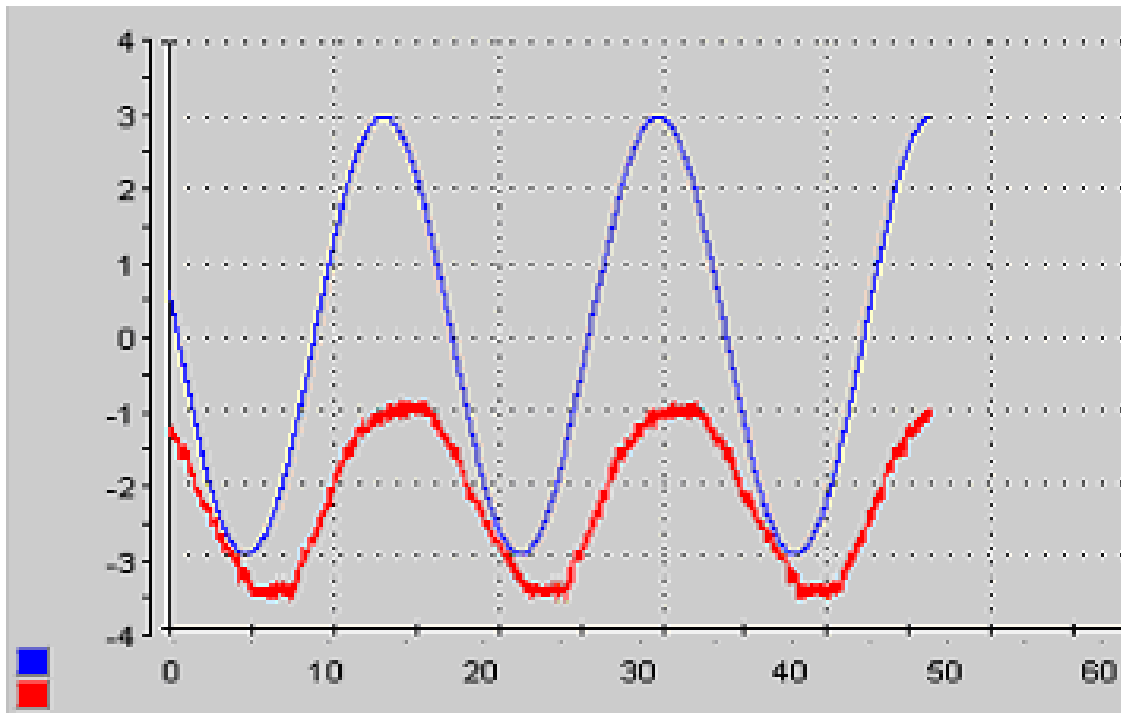


Figure 4.10. Adaptive Controller in (4.4) result with $\gamma = 1$. Desired input position is a sinusoid with amplitude=3, and frequency=0.06Hz. Time in (s) versus actual position (red) and desired position (blue) in (mm).

Using same adaptation law in (4.5) and refinement of the PID adaptive controller to be dependent on the error signal as the signal vector that will be multiplied to all controller parameters i.e. $\mathbf{v}(t)=[e \quad \dot{e} \quad e]^\top$ leads to a new enhanced version of the PID adaptive controller in figure 4.9.

Figure 4.11 shows the results of testing the enhanced PID adaptive controller with the error signal as the signal vector for all controller parameters. Appendix B14 shows the SIMULINK model of the enhanced PID adaptive controller used.

A snapshot of the experiment run in dSPACE showing the adaptation coefficient and the adaptation parameters K_p , K_i , and K_d in figure C.4 appendix C.

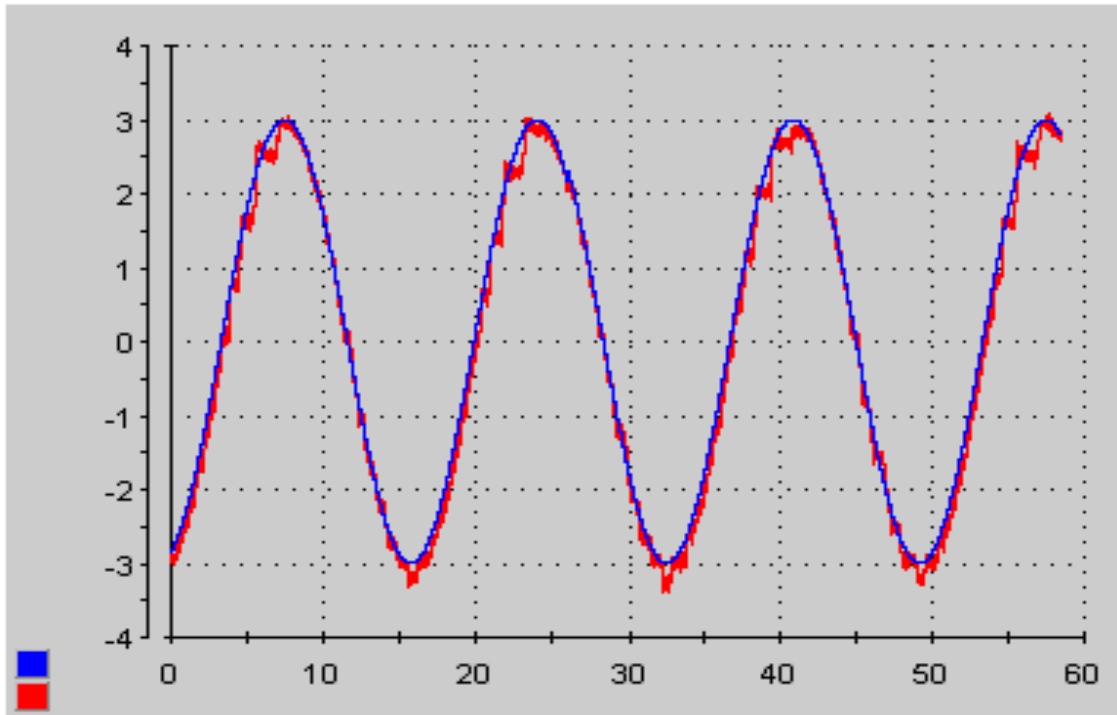


Figure 4.11. Enhanced PID Adaptive Controller results, all adaptive PID parameters multiplied by the error signal vector with $\gamma = 1$. Desired input position is a sinusoid with amplitude=3, and frequency=0.06Hz. And controller adaptive coefficients K_p , K_i , and K_d are 119, 0.88, and 0.031 respectively. Time in (s) versus actual position (red) and desired position (blue) in (mm).

To remove the ripples shown above, *Step2* is done to build the PID adaptive controller with adaptation law in (4.5) that's tested and shows excellent results in controlling the position of the SMA.

Figure 4.12 shows the position control results of the PID adaptive controller with excellent performance, note that there is a time interval needed for adaptation. Also note that the signals here are cleaner and smoother than the signals in figure 4.11 but there is a delay between the desired signal and the actual signal.

Multiple set of experiments show that the PID adaptive controller with error vector signal is an enhanced PID adaptive controller with more consistency and less adaptation time.

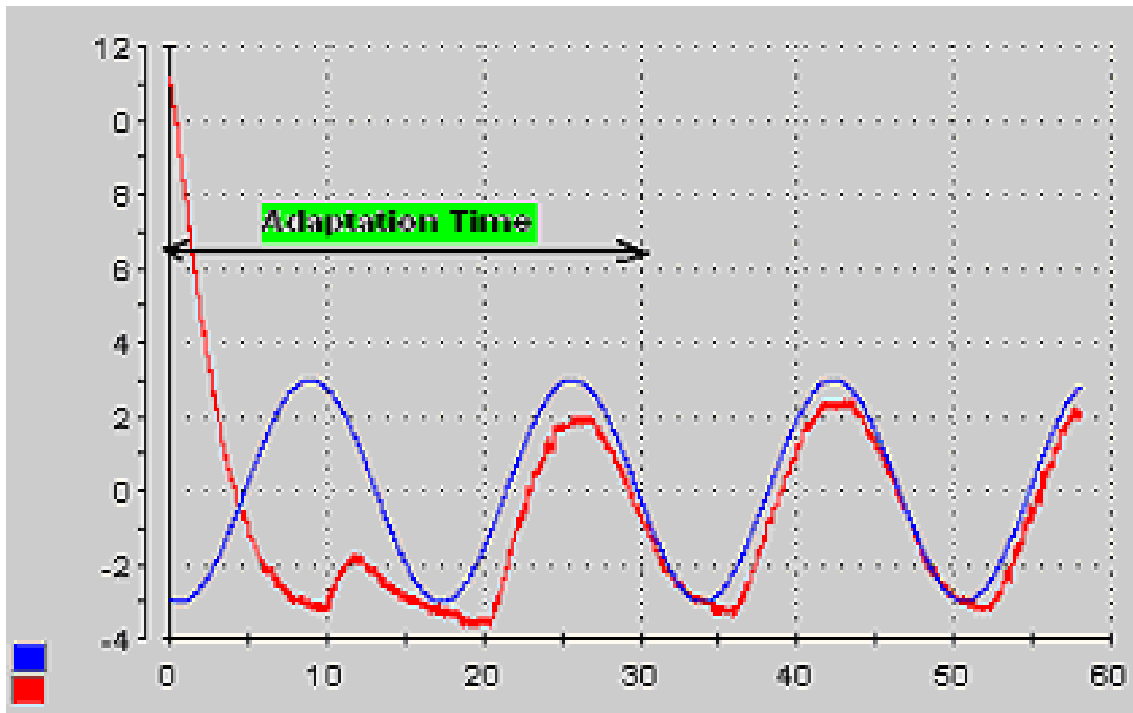
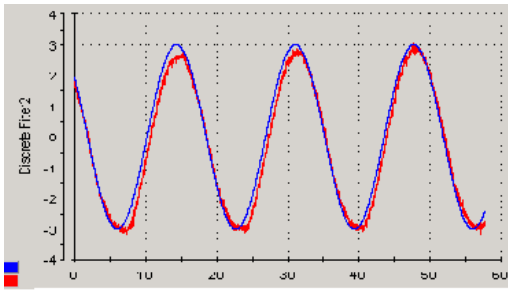


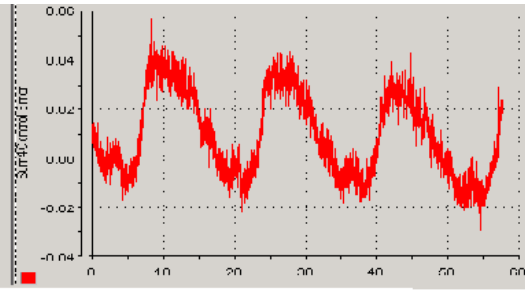
Figure 4.12. PID Adaptive Controller, with $\gamma = 1$. Desired input position is a sinusoid with amplitude=3, and frequency=0.06Hz. Time in (s) versus actual position (red) and desired position(blue) in (mm).

:Changing the desired position Frequency .4.3.4.1

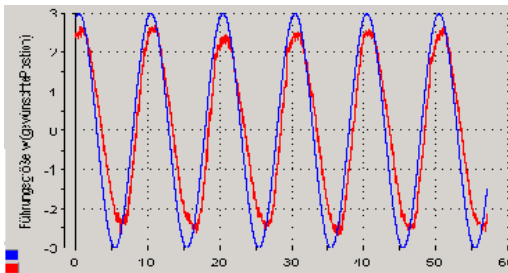
Figure 4.13. shows the results of testing the enhanced PID adaptive controller in Appendix B14 under different frequencies of the desired position.



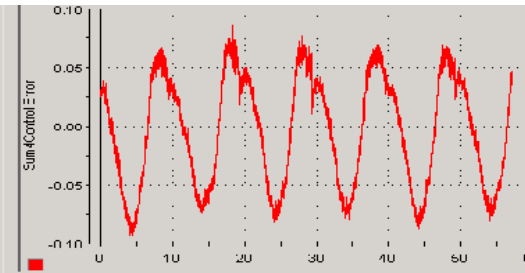
(a.1) Actual Position and Desired position at $f=0.06$ Hz



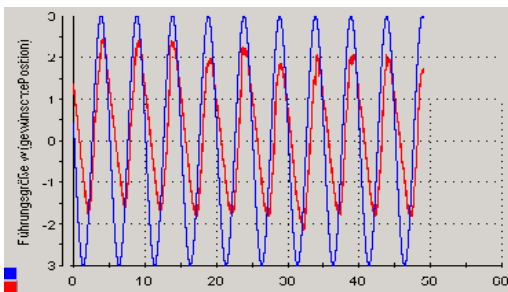
(b.1) Control Error at $f=0.06$ Hz



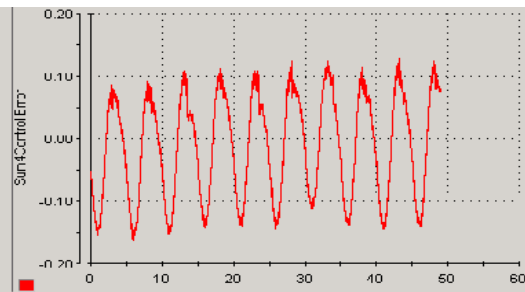
(a.2) Actual Position and Desired position at $f=0.1$ Hz



(b.2) Control Error at $f= 0.1$ Hz



(a.3) Actual Position and Desired position at $f= 0.2$ Hz



(b.3) Control Error at $f= 0.2$ Hz

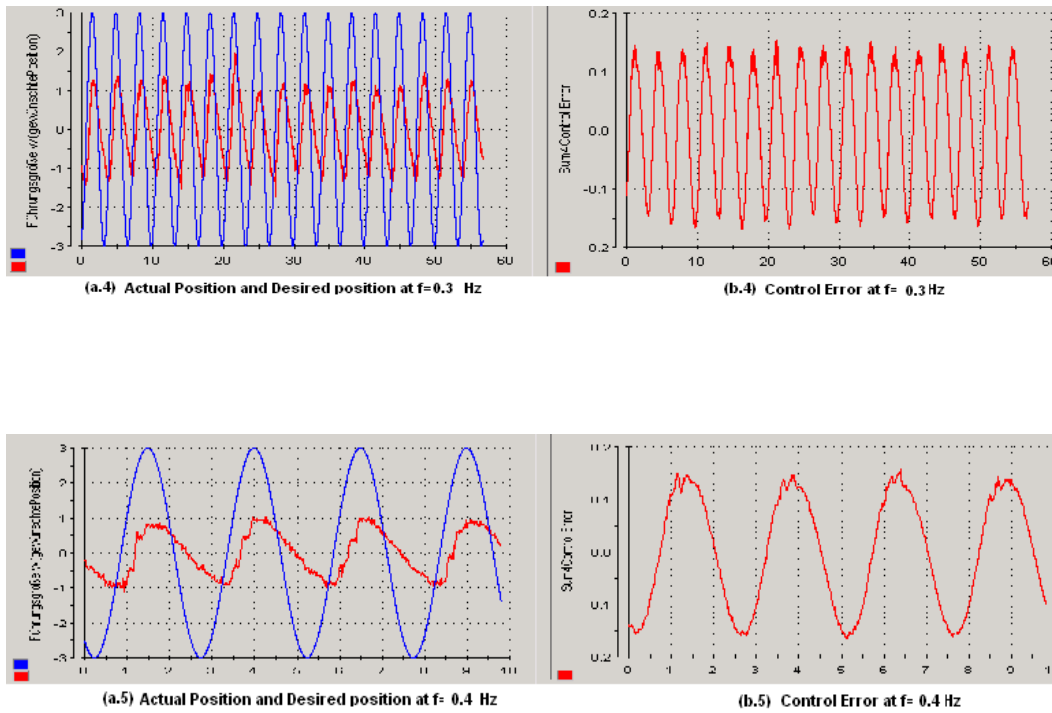


Figure 4.13. Enhanced PID Adaptive Position Controller Results with $\gamma=1$. Desired input position is a sinusoid with amplitude=3. (a.1) to (a.5) Time in (s) versus actual position (red) and desired position (blue) in (mm). (b.1) to (b.5) Time in (s) versus control error under different frequencies of desired position.

:Changing the adaptation coefficient .4.3.4.2

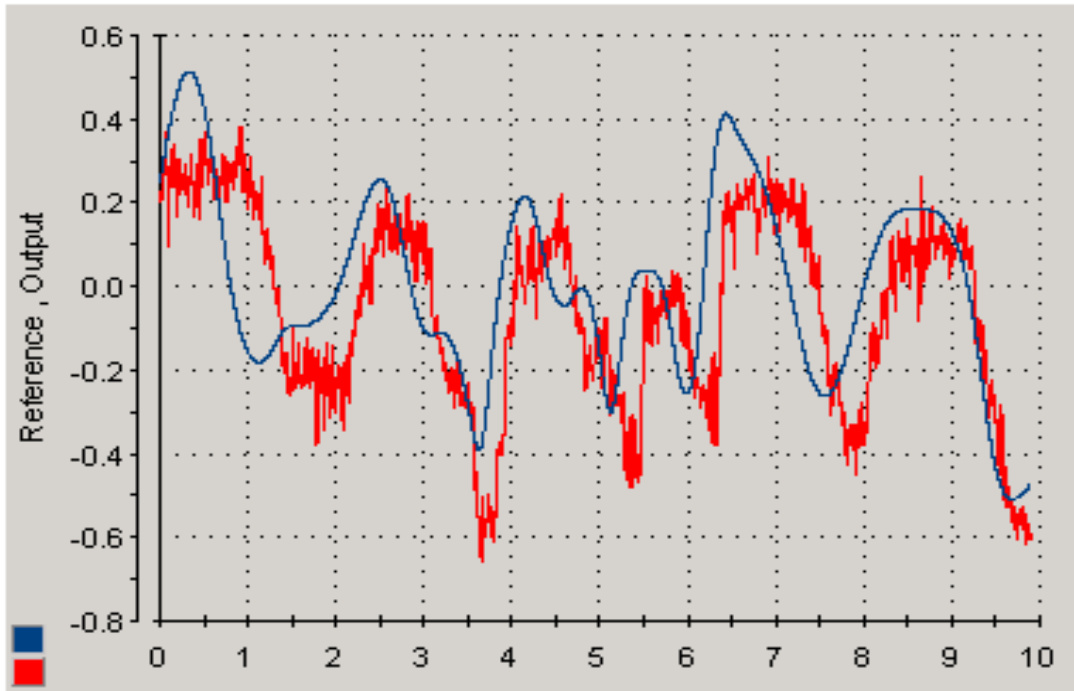
Table C.5. appendix C shows the experimental results of position control error under different sets of adaptation coefficients $\gamma= (1, 0.5, \text{ and } 0.3)$, for this plant it's proved that for $\gamma=1$ under different sets of experiments it gives the best performance, any increase or decrease will affect the performance of the adaptive controller.

The online K_p , K_i , and K_d parameters running the PID adaptive control under different sets of adaptation coefficients gives the following values for the PID gains $K_p= [13.2-13.9]$; $K_i = [0.3;1]$; and for $K_d=[0.33;0.39]$. So, these values can be used for tuning a PID controller with coefficient's ratios $[K_p: K_i: K_d] = [14:1:0.3]$. Then, this adaptive controller can be used to tune the K_p , K_i and K_d coefficients for any linear or nonlinear plant with unknown dynamics.

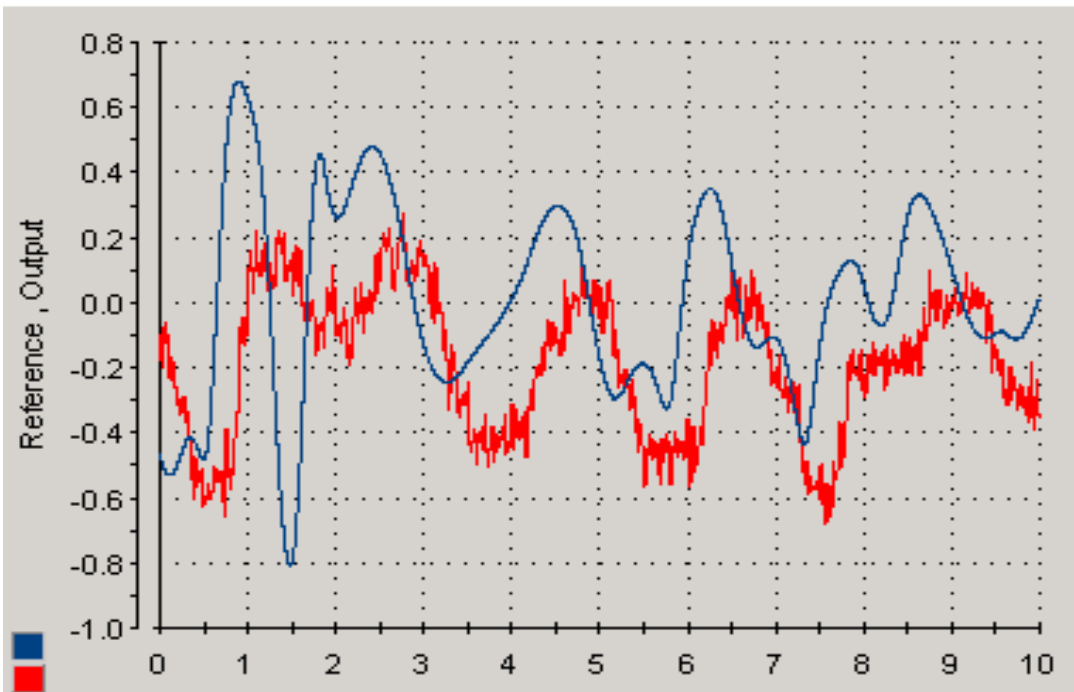
However, multiple set of experiments have shown that the enhanced PID adaptive controller in figure C.4 appendix C is more consistent than the PID adaptive controller in figure 4.9. And its best results are seen at $\gamma=0.3$ with $[K_p, K_i, K_d] = [2.5, 108, 0.095]$.

:Using Chaotic Wave Signal Input .4.3.4.3

Figure 4.14 shows the results of using an arbitrary chaotic signal as the desired position for both the PI controller and the PID adaptive controller. The chaotic signal is generated using the Chua's equations set [24]. Appendix B15 shows the SIMULINK model used to generate this signal. The performance of both controllers is very good with few delays in the actual position, but the overall performance of the PI controller is better. The reason for testing a chaotic wave signal as the desired position is to check the robustness of the non model-based controllers in the case of an arbitrary signal input which is unlike the sinusoidal consistent form. Especially for the case of PID adaptive controller that shows that its adaptability is not mainly based on the input signal consistency, while it's more dependent on the plant dynamics and the error signal.



(a) PI Controller Result using chaotic desired position.



(b) PID Adaptive Controller Result using chaotic desired position, $\gamma=3$.

Figure 4.14. PI and enhanced PID adaptive controller results using chaotic signal as the desired position. Time in (s) versus desired position (blue) and actual position (red) in (mm).

4.4. Conclusions on the non model-based approach

The non model-based approach using tuned PI controller and PID adaptive control shows its success and robustness to control the position of the SMA wire. Compared to model-based and behavioral-based approaches, it's easier to implement, and more successful as it is not temperature dependant, while requires few manual tuning and calibration of the system mechanics or position offset signal in some times.

Comparing the results of the PID adaptive controller in figure 4.9 with the enhanced PID adaptive controller in figure C.4 appendix C. The second is more consistent, which shows that tuning and experimental trial and error is the best way to have a consistent control.

Comparing the performance of the PI controller to that of the PID adaptive control, the following is proved by experiment:

1. The performance of the PI position controller is better and with small control error difference of [0.1-1] mm ranges than in the PID adaptive control under different sets of desired position frequencies.

2. PI and PID adaptive controller both have decreased performance at frequencies higher than 0.1 Hz due to the normal behavior of the SMA especially in the natural cooling region which needs about 20 sec for heat convection.

3. PID adaptive controller has the benefit over PI that the control error reaches a fixed limit of [-3, 3] mm increasing the frequency of the desired position. While for PI controller the control error keeps increasing. Figure 4.15. shows the performance of the PI and PID adaptive controllers under different frequencies.

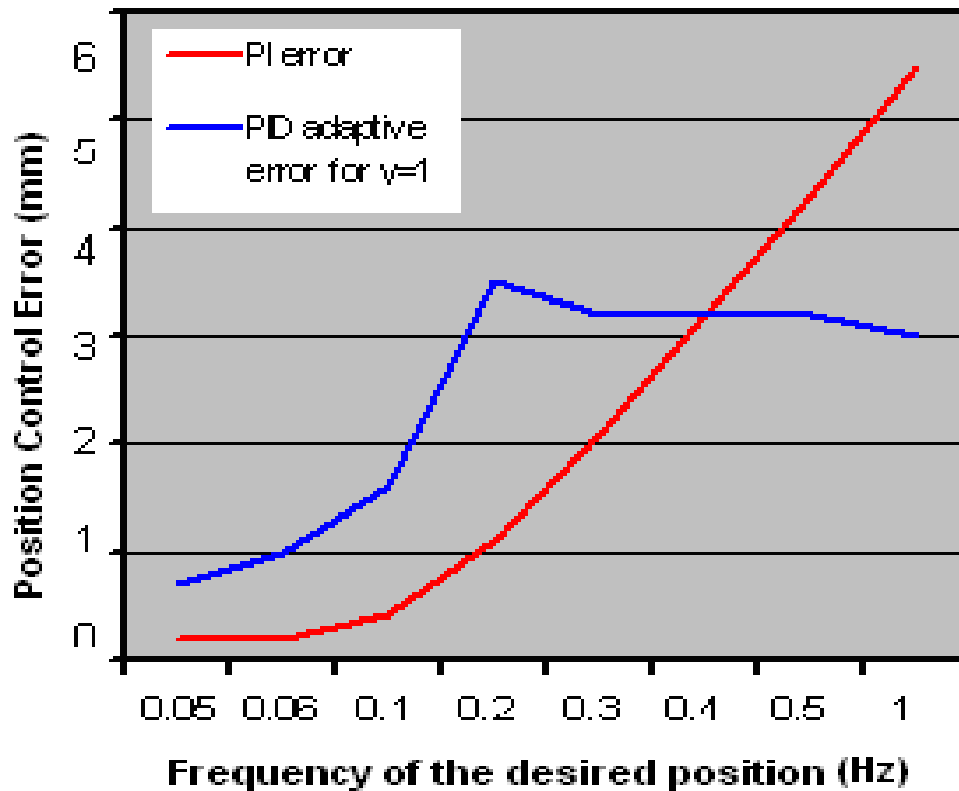


Figure 4.15. Position Control Error of PI and PID adaptive controller under different frequencies of the desired position.

4. Another advantage for the PID adaptive controller that the monitored K_p , K_i , K_d parameters can be used to tune a regular PID controller to control the system. On the other hand, the values doesn't reach the experimental tuned PI controller gains which are $K_p=250$ and $K_i=20$ and this will also lead to the conclusion that this adaptive concept can be used just for first step of tuning while more manual tuning of the controller to fit the system plant changes is still needed.

Chapter 5

Results and Conclusion

5.1. Conclusion

The SMA hysteretic behavior under changes of the excitation frequency, amplitude of the current input signal, and the load attached to the SMA wire shows its main dependency on the frequency of the input signal, proved in Chapter 2 through a set of experiments. The usage of this hysteretic shape memory behavior is required in the usage of this SMA as an actuator and that's why a position controller is needed for the SMA.

The model- and behavioral-based approaches developed in Chapter 3 in three different models the AM, V, and O models that cannot be validated due to their dependency on the wire temperature form a basis for future research in building a generalized behavioral-based model for the shape memory alloy. And since the problem is in different behaviors from different configurations of the SMA even with same NiTi material, the concern is not only to be able to use the SMA as an actuator in different systems, but also to allow using it in other applications, and that's why a model of the SMA material is required to understand its interaction and contribution in any systems dynamics in general. The contribution of this research in the part of behavioral modeling of the SMA since it's the first research in SMAs to tackle the usage of the heat transfer equation as the behavioral model, to discuss a non-passivity of the material, to consider the effect of volume change in the SMA material, and to control by characteristic parameter change as done in the model-based controller using the resistance as the parameter.

However, the non model-based approaches derived in Chapter 4 in two different controllers the PI and the adaptive PID lead to a robust position control of the shape memory alloy wire. The advantage of this approach that it is not temperature dependant and could be used in any type of SMA wires with few tuning of the parameters and calibration of the system.

Furthermore, the PID adaptive controller derived in this research by mathematical methods and enhanced by experimental trial and error using the error signal as the vector signal of all PID adaptive parameters can be used to control any linear or non-linear plant with unknown dynamics with high consistency. However, it can also be used to tune the gains of a regular PID controller.

5.2. Motivation and Future Work

Although all the non model- and behavioral-based approaches could not be validated due to its dependency on the temperature of the wire, but it can be used on further research to test it under variable temperature function of the SMA; which needs another research on building temperature identification of the SMA in terms of the material coefficients and dimensions, hence a refinement of the heat transfer equation in terms of all temperature dependant variables will be needed.

However, as a motivation of this research, a lot of applications that need a fast actuator can use the SMA. Another suggestion as a future research for using the SMA material in telecom applications like in smart antennas. In this case, the SMA required is an SMA plate so that to control the coverage area and orientation of the antenna beams for main lobes or side lobes under different criteria's like in adaptive antennas based on the change of the shape of the plate embedded in or joint to the antenna receiver-transmitter unit.

References

- [1] R. Velazquez, E. Pissaloux, M. Hafez, and J. Szewczyk, "Measurement of SMA Thermal Properties in the Design/Evaluation of Actuators", Laboratoire de Robotique de Paris, Universite Paris, 2005.
- [2] Sushant M. Dutta, Fathi H. Ghorbel, "Differential Hysteresis Modeling of a Shape Memory Alloy Wire Actuator", IEEE/ASME Transactions on Mechatronics, Vol. 10, No.2, 2005.
- [3] D.R. Reynolds, "A Nonlinear Thermodynamic Model of Phase Transitions in Shape Memory Alloy Wires", Ph.D. Thesis, Rice University, Houston, TX, May, 2003.
- [4] Seelecke S., "Adaptive Structures with SMA Actuators - Modeling and Simulation, Habilitation thesis", TU Berlin, 1999.
- [5] A. Falvo, "Thermomechanical characterization of Nickel-Titanium Shape Memory Alloys", Dottorato di ricerca - XX ciclo - Università della Calabria, 2007.
- [6] Shibly, H. and Söffker, D., "Mathematical model of shape memory alloy wire using experimental data", MCMDS-Journal of Mathematical and Computer Modeling of Dynamical Systems, Submitted.
- [7] J. E. Bidaux, L. Bataillard, J. A. Son, and R. Gothardt, "Phase Transformation Behavior of thin shape memory alloy wires embedded in a polymer matrix composite", Journal de Physique IV, 1993.
- [8] Masanari Tomozawa, Hee Young Kim, and Shuichi Miyazaki, "Microactuators using R-phase transformation of sputter-deposited Ti-47.3Ni shape memory alloy thin films", Journal of Intelligent Material Systems and Structures, Vol. 17, 2006.
- [9] H. Jonacha, "Actuators Basics and Applications", p. 241-245, © Springer Berlin Heidelberg New York, 2004.

[10] W.J. Buehler and F.E.Wang., "A summary of recent research on the nitinol alloys and their potential application in ocean engineering". *Ocean Eng.*, 1:105–120, 1967.

[11] Haroun Mahdavi, S. and Bentley, P. J., "Evolving Noise Tolerant Antenna Configurations using Shape Memory Alloys", In Proc of the Second International Conference on Computational Intelligence, Robotics and Autonomous Systems, Singapore, 2003.

[12] Heinrich Kötter, "Construction of an intelligent actuator Test Rig for the SMA", Seminar Paper, Institute for Mechatronics and System Dynamics, SRS, University of Duisburg-Essen, Germany, 2003.

[13] Yu, Qing, "Experimental Identification of the Dynamic Hysteresis of Shape Memory Wires", Bachelor's Thesis, University of Duisburg-Essen, Germany, 2005.

[14] DS1104 R&D Controller Board, "Installation and Configuration Guide", For Release 3.4, For DS1104 and CP1104/CLP1104 Connector Panels, dSPACE, 2005.

[15] ControlDesk, "Experiment Guide", For Release 3.4, dSPACE, 2005.

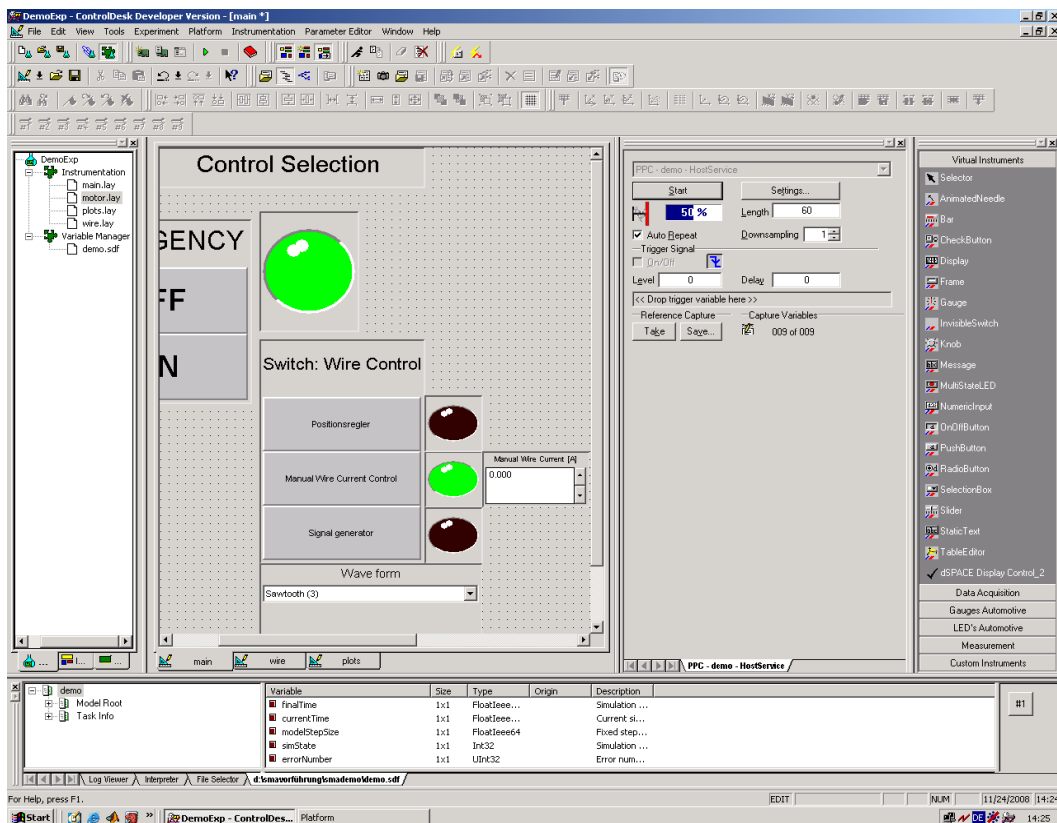
[16] C. Liang and C. Roger, and M. Buisson, "One-dimensional Thermomechanical constitutive relations for shape memory materials", *Journal of Intelligent Materials, Systems and Structures*, Vol. 1, No. 2, 1990.

[17] Yee Harn Teh, and Roy Featherstone, "A new control system for fast motion control of SMA actuator wires", Dept. Of Systems Engineering, Research School of Information Sciences and Engineering, The National University, 2003.

- [18] G. Song, V. Chaudhry, and C. Batur, "Precision tracking control of shape memory alloy actuators using neural networks and a sliding-mode based robust controller", Institute of Physics Publishing, Smart Materials and Structures, Vol. 12, 2003.
- [19] N. Bizdoaca, H. Hamdan, and D. Selisteanu, "Fuzzy Logic Controller for a Shape Memory Alloy Tentacle Robotic Structure", University of Craiova, Romania, IMRAC, France, 2006
- [20] Gene F. Franklin, J. David Powell, and Abbas Emami-Naeini, "Feedback Control of Dynamic Systems", Fifth Edition, p186-189, ©2006 by Pearson Education Inc.
- [21] Katsujiko Ogata, "Modern Control Engineering", Forth Edition, p 682-685, ©2002 by Prentice Hall, Inc.
- [22] Slontine and Li, "Applied Nonlinear Control", p 312-328, ©1991 by Prentice Hall International Inc.
- [23] Fiang Li, Robert D. Brandt, and George Saikalis, "Self Tuning of PID Controllers by Adaptive Interaction", Proceedings of the American Control Conference, Chicago, IL, 2000.
- [24] Al-Sweiti, Y. M., "Modeling and Control of an Elastic Ship-Mounted Crane Using Variable-Gain Model-Based Controller", PhD. Thesis, University of Duisburg-Essen, Germany, 2006.
- [25] SMA/MEMS Research Group, "SMA Memory Alloys: Microscopic Diagram of the Shape Memory Effect", Oulu University, <http://www.cs.ualberta.ca> , Aug, 17, 2001
- [26] Alumni of Thermodynamics, "Shape Memory Alloy: Applications", Technical University of Berlin, <http://www.smaterial.com> , Aug, 8, 1996.

APPENDIX- A
SOFTWARE AND MATLAB CODE

A.1. dSPACE ControlDesk Software User Interface



A.2. Heat Transfer Function MATLAB Code

% ***Heat Transfer Equation Solution Using Runge Kutta 4th Order Method

% ***to find the Temperature of the SMA wire

% ***Loaded data files data0xx.mat are saved from the dSPACE experiments

clear all

close all

%-----

% Physical Values

%-----

r=0.1525e-3;

l=0.525;

A=2*pi*r*l;

v=pi*r*r*l;

R=4;

```
ro=6450;
cp=1350;
h=150;
tau=(ro*cp*v)/(h*A);
D=R/(h*A);
load data013
%-----
% Raw Data Reading
%-----
time=data013.X.Data;
y1=data013.Y(:,1).Data;
y2=data013.Y(:,2).Data;
y3=data013.Y(:,3).Data;
y4=data013.Y(:,4).Data;
y5=data013.Y(:,5).Data;
y6=data013.Y(:,6).Data;
y7=data013.Y(:,7).Data;
%-----
figure
subplot(3,3,1)
plot(time,y1)
ylabel('Force')

subplot(3,3,2)
plot(time,y2)
ylabel('Room Temperature')

subplot(3,3,3)
plot(time,y3)
ylabel('Motor Current')

subplot(3,3,4)
plot(time,y4)
ylabel('Wire Current')
```

```
subplot(3,3,5)
plot(time,y5)
ylabel('Actual Position')

subplot(3,3,6)
plot(time,y6)
ylabel('Desired Position')

subplot(3,3,7)
plot(time,y7)
ylabel('Position Deviation')
N2=size(time)
%-----
% Data Filtering
%-----
figure % draw data after filering
[f11,f22]=butter(2,0.05);
y1=filter(f11,f22,y1);

subplot(3,3,1)
plot(time,y1)
ylabel('Force')
[f11,f22]=butter(2,0.025);
y2=filter(f11,f22,y2);

subplot(3,3,2)
plot(time,y2)
ylabel('Room Temperature')
[f11,f22]=butter(2,0.005);
y3=filter(f11,f22,y3);

subplot(3,3,3)
plot(time,y3)
```

```
ylabel('Motor Current')
```

```
[f11,f22]=butter(2,0.005);
```

```
y4=filter(f11,f22,y4);
```

```
subplot(3,3,4)
```

```
plot(time,y4)
```

```
ylabel('Wire Current')
```

```
[f11,f22]=butter(2,0.05);
```

```
y5=filter(f11,f22,y5);
```

```
subplot(3,3,5)
```

```
plot(time,y5)
```

```
ylabel('Actual Position')
```

```
[f11,f22]=butter(2,0.05);
```

```
y6=filter(f11,f22,y6);
```

```
subplot(3,3,6)
```

```
plot(time,y6)
```

```
ylabel('Desired Position')
```

```
[f11,f22]=butter(2,0.05);
```

```
y7=filter(f11,f22,y7);
```

```
subplot(3,3,7)
```

```
plot(time,y7)
```

```
ylabel('Position Deviation')
```

```
elong=508.2-y5;
```

```
sh=[time;y1;y2;y3;y4;elong;y6;y7];
```

```
save sh sh
```

```
Tr=mean(y2)
```

```
To=Tr;
```

```
%-----
```

```
% Solution of the Differential Equation
```

```
%  $\tau(dT/dt)+T=Di^2+Tr$ 
```

```
% where  $\tau=ro.cp.v/hA$ ,  $D=R/hA$ 
```

```
%Runga-Kutta 4-th order Method
```

```
%-----
```

```
h1=0.01;
```

```
w(1)=Tr;
```

```
Tw(1)=Tr;
```

```
%dummy1=w(1);
```

```
N1=length(time);
```

```
for i=2:N1
```

```
    t=time(i);
```

```
    cur=y4(i);
```

```
    k1=h1*func2(tau,D,Tr,cur,t,w(i-1));
```

```
    k2=h1*func2(tau,D,Tr,cur,t+0.5*h,w(i-1)+0.5*k1);
```

```
    k3=h1*func2(tau,D,Tr,cur,t+0.5*h,w(i-1)+0.5*k2);
```

```
    k4=h1*func2(tau,D,Tr,cur,t+h,w(i-1)+k3);
```

```
    dummy=(k1+2*k2+2*k3+k4)/6;
```

```
    w(i)=w(i-1)+dummy;
```

```
    Tw(i)=w(i);
```

```
    t=t+h1;
```

```
end
```

```
figure
```

```
y55=y5+18;
```

```
y5max5=max(y55);
```

```
for i=1:N1
```

```
    strain(i)=(y55(i))/525;
```

```
end
```

```
plot(time,y55)
```

```
grid on
```

```
figure
```

```
yy4=100*y4;
```

```
elo=10*y55;
```

```
plot(time,Tw,time,elo,time,yy4)
```

```
grid on
```

```
figure
```

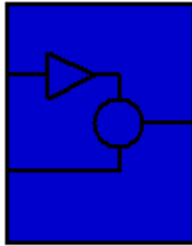
```
plot(Tw,strain)
```

```
axis([0,120,0,0.04]);  
grid on  
xlabel('Temperature [deg]')  
ylabel('Strain')
```

APPENDIX- B ***SIMULINK MODELS***

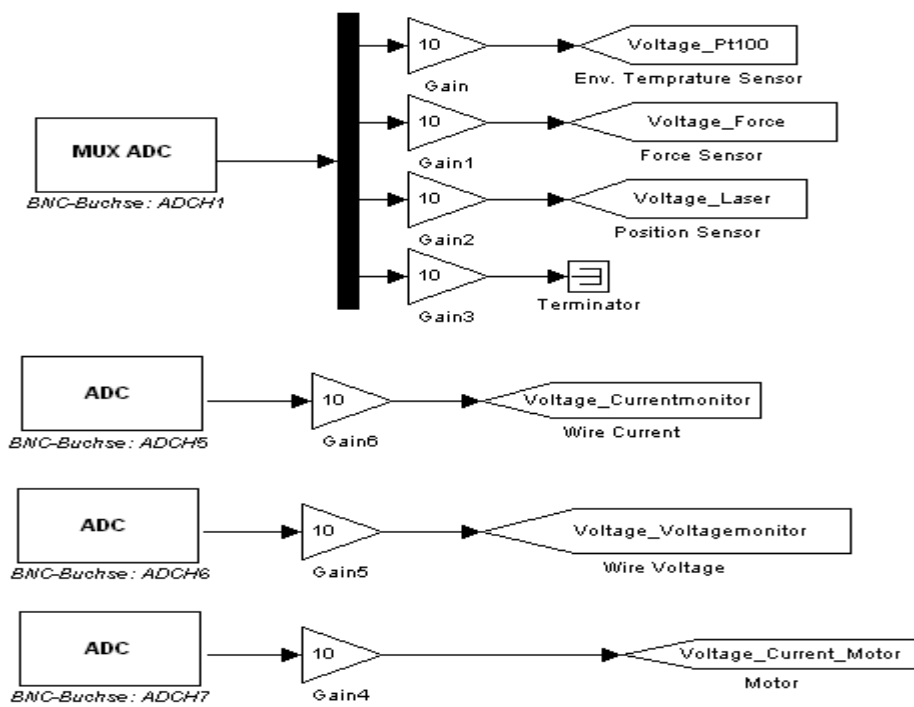
B1. SIMULINK RTI-DSPACE Interface to the SMA Test Rig

B1.1. Input from Test Rig to dSPACE SIMULINK subsystem

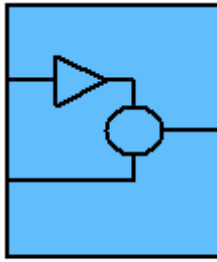


INPUT &
SYSTEMGAIN

B1.1.1. Masked Blocks under INPUT & SYSTEM GAIN

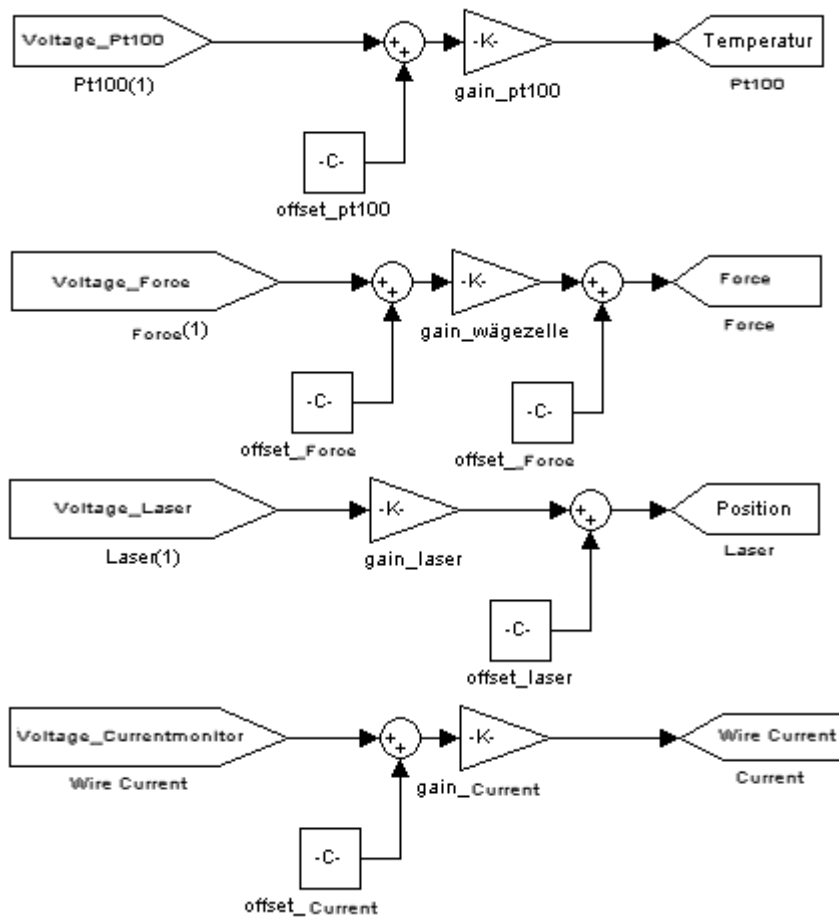


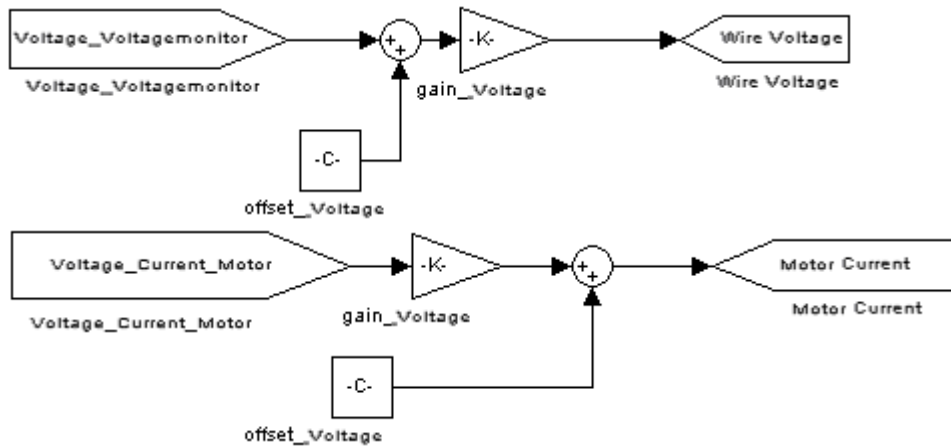
B2. Inputs data conversion SIMULINK subsystem



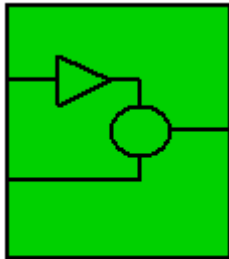
INPUT VALUE
CONVERSION

B2.1. Masked blocks under INPUT VALUE CONVERSION



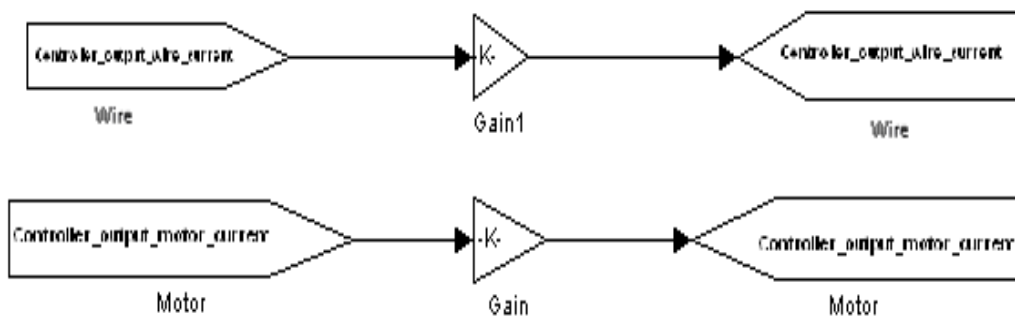


B3. Output data conversion SIMULINK subsystem.

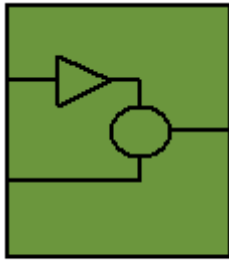


OUTPUT VALUE
CONVERSION

B.3.1. Masked blocks under OUTPUT VALUE CONVERSION

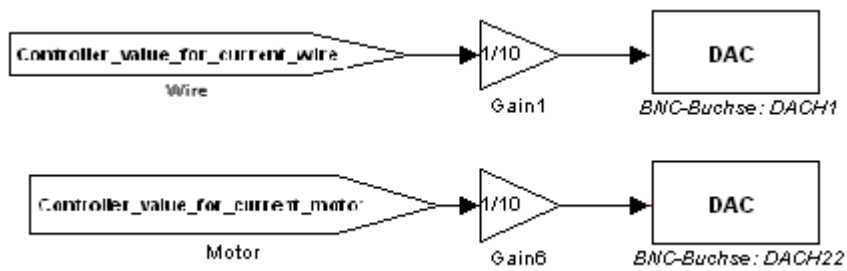


B.4. Output from PC to dSPACE control box SIMULINK subsystem.

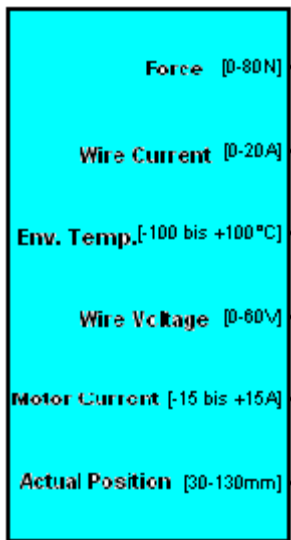


OUTPUT &
SYSTEMGAIN

B4.1. Masked blocks under OUTPUT & SYSTEM GAIN

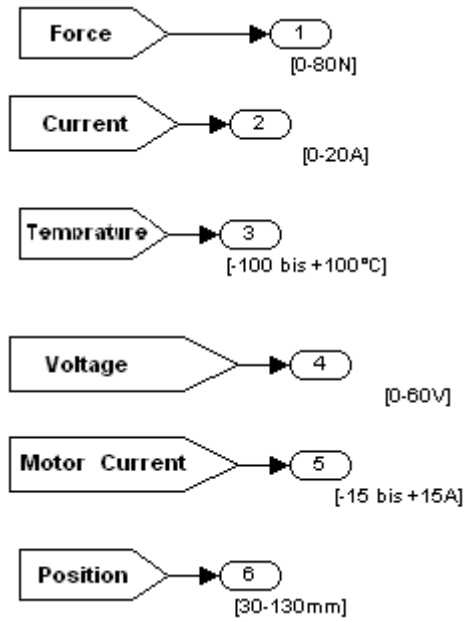


B5. Input to Controller Simulink Subsystem

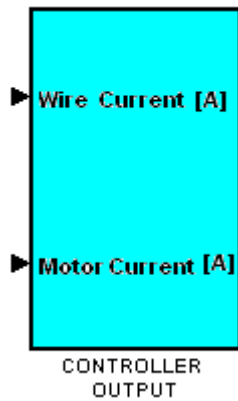


CONTROLLER INPUT

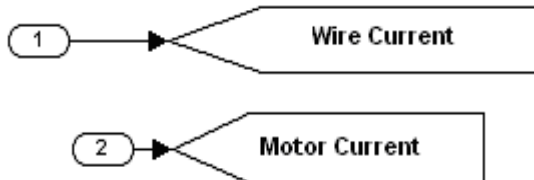
B5.1. Masked blocks under CONTROLLER INPUT



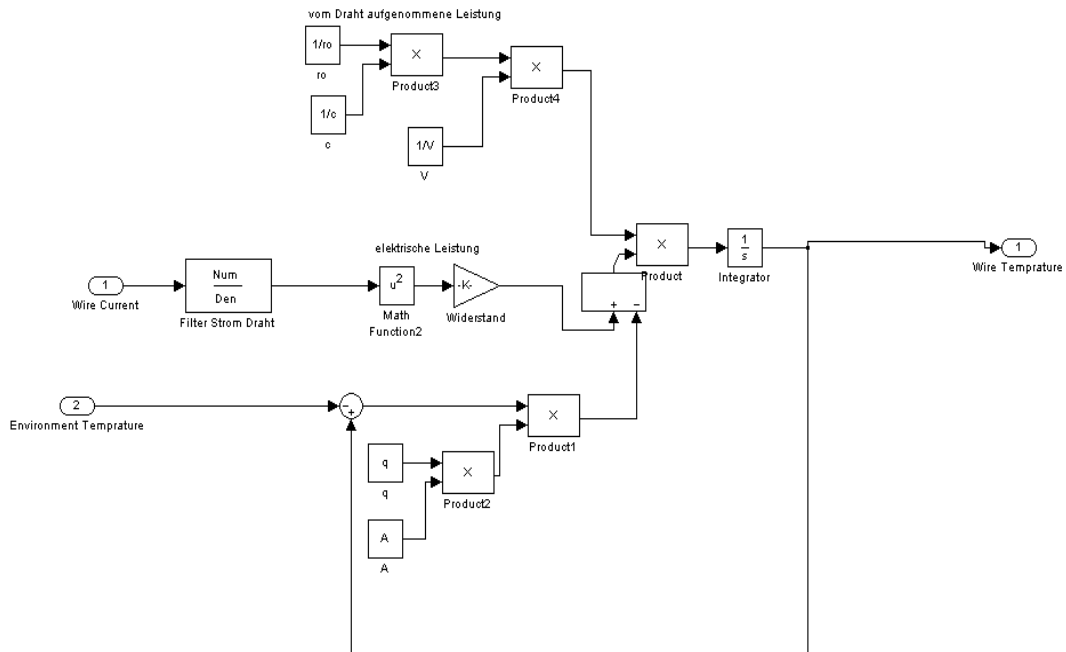
B6. Output of the Controller SIMULINK Subsystem



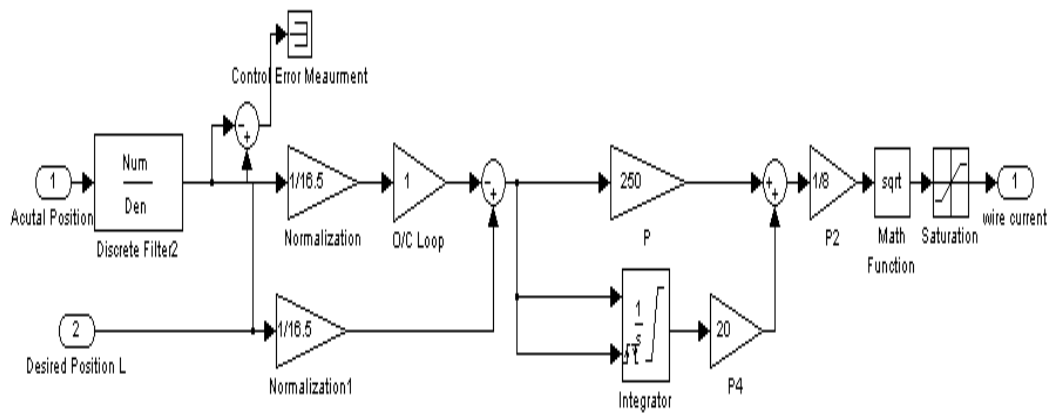
B6.1. Masked blocks under the CONTROLLER OUTPUT



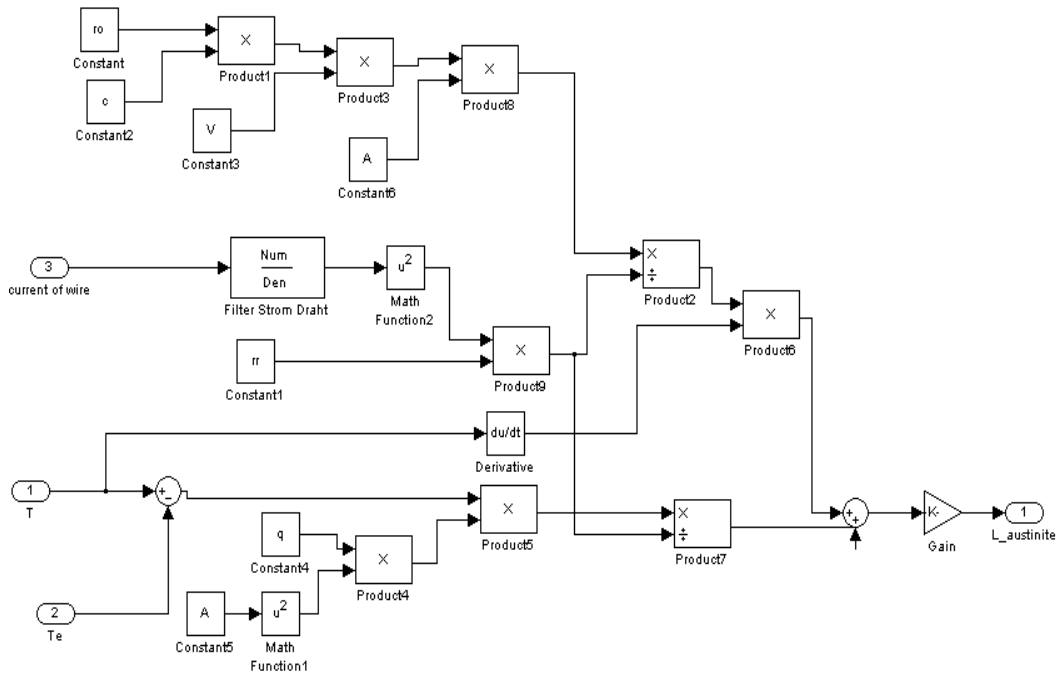
B7. Masked blocks under the Heat Transfer Equation SIMULINK subsystem



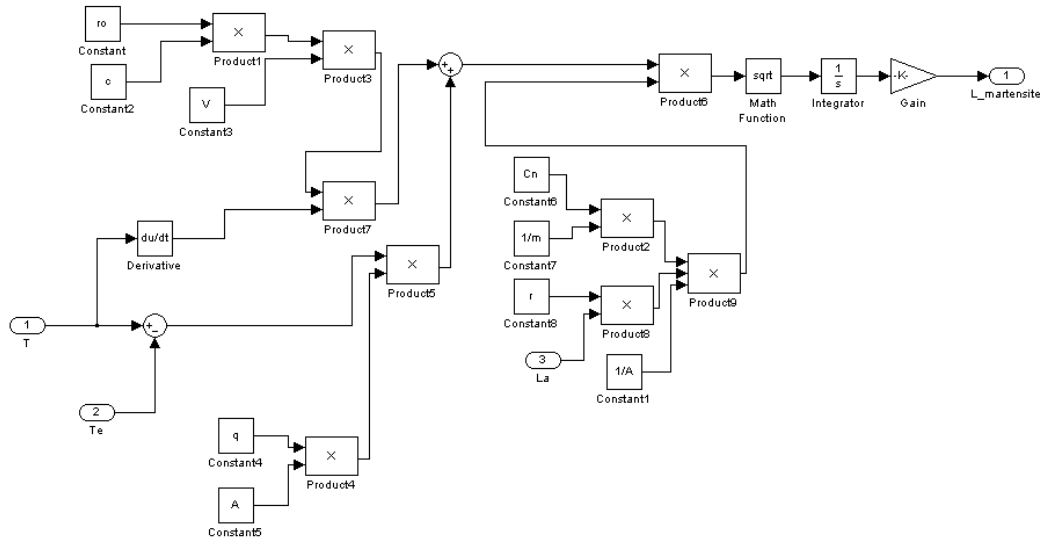
B8. Masked blocks of the PI Controller SIMULINK subsystem



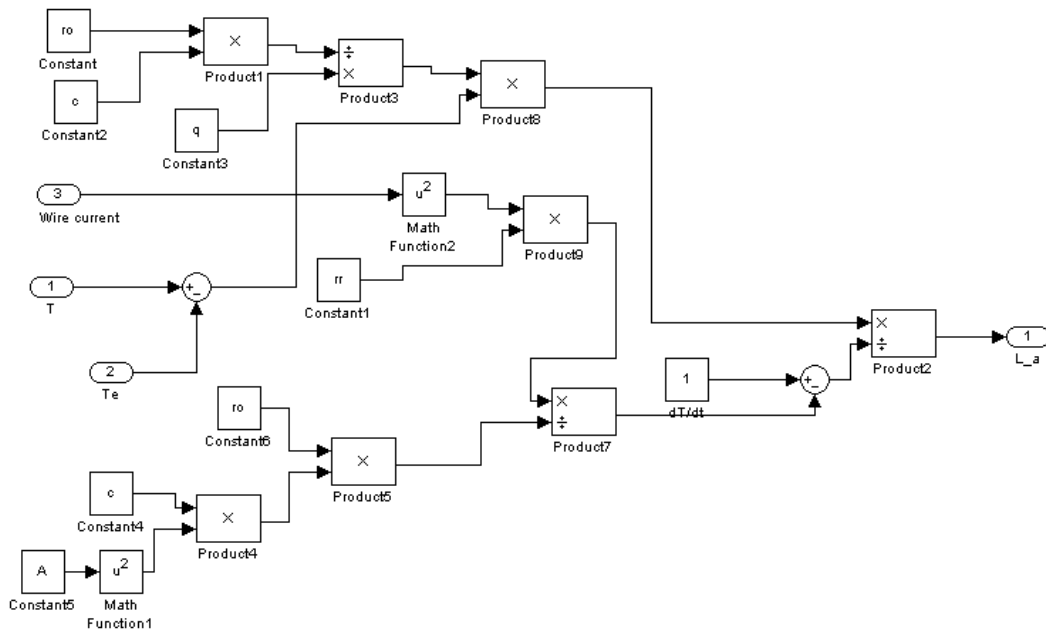
B9. Masked blocks under the Austinite SIMULINK subsystem



B10. Masked blocks under the Martensite SIMULINK subsystem

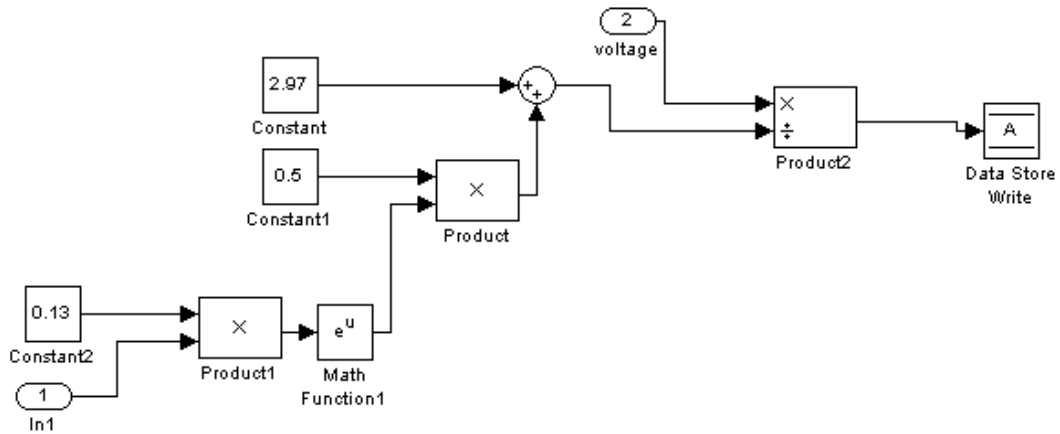


B11. Masked blocks under the V-Model SIMULINK subsystem

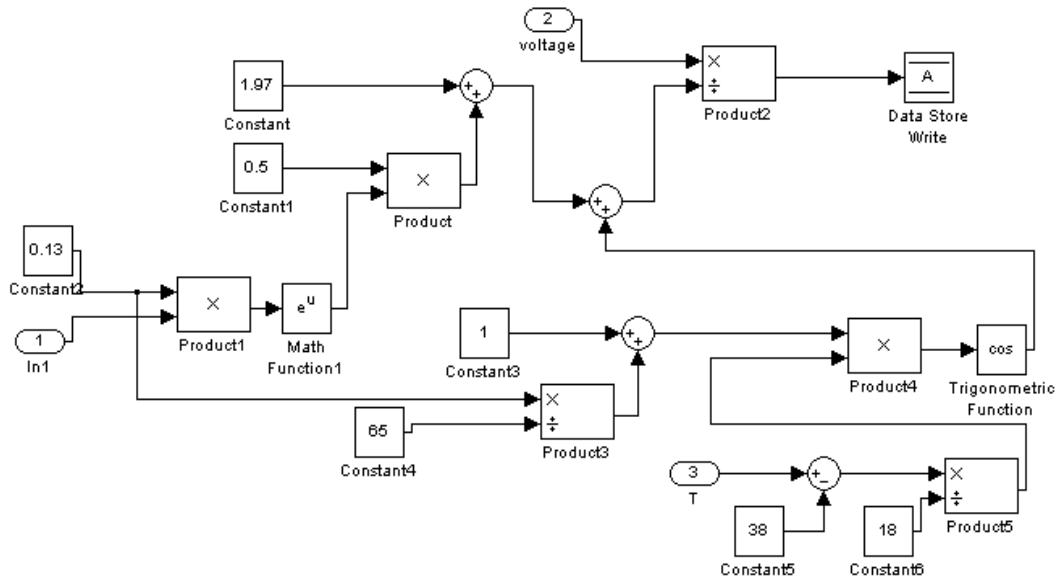


B12. Masked blocks under the austinite resistance of the Ohm-Model SIMULINK subsystem

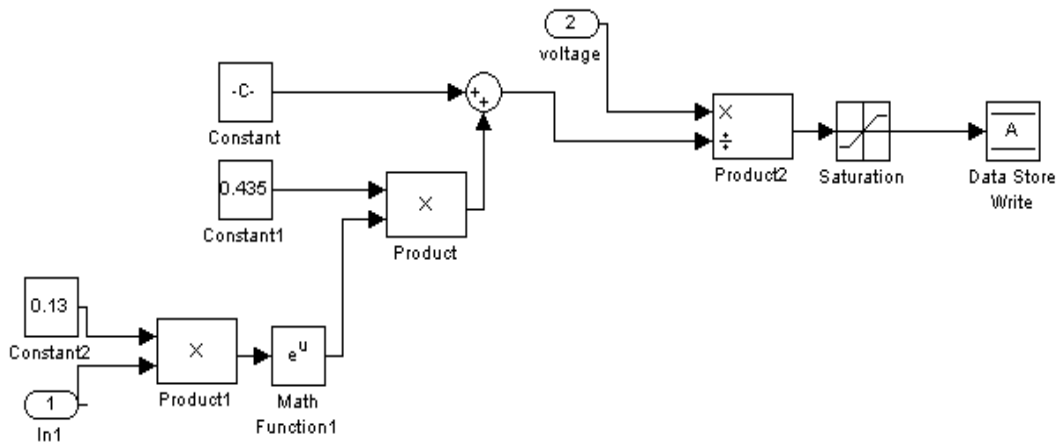
B12.1 Austinite R1



B12.2. Austinite R2

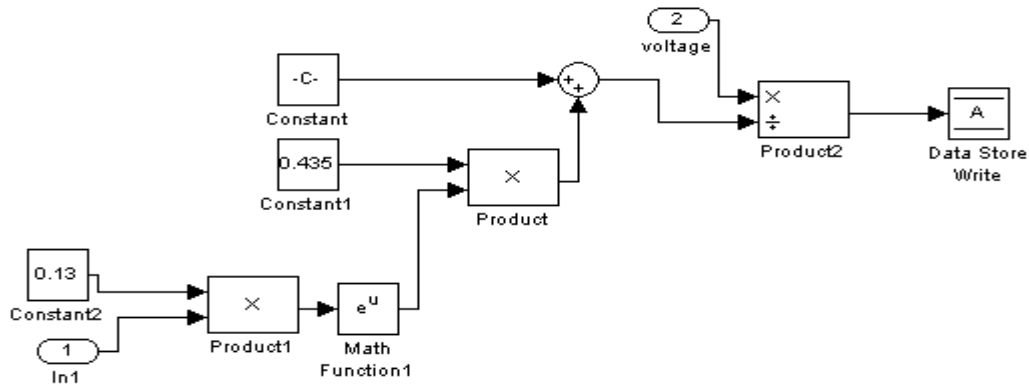


B12.3. Austinite R3

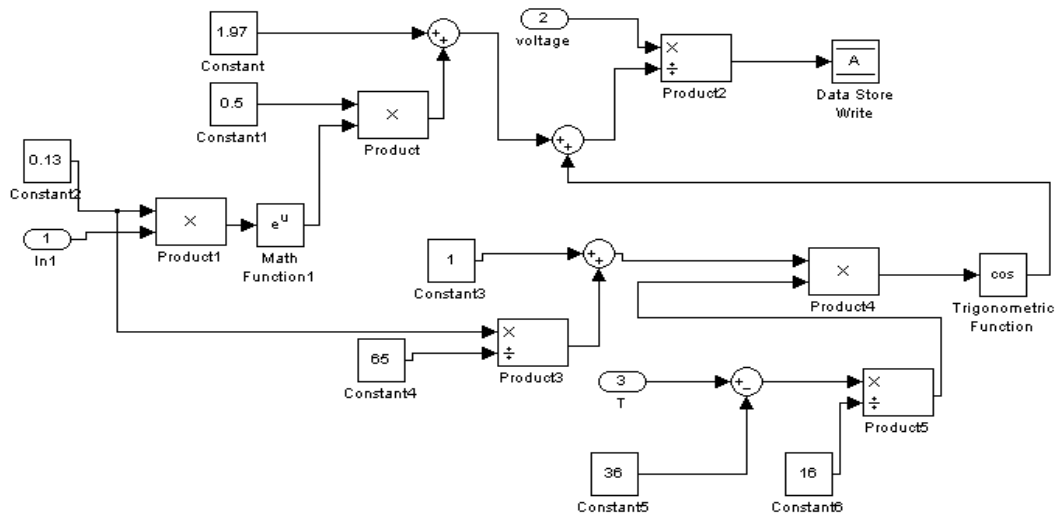


B13. Masked blocks under the martensite resistance of the Ohm-Model SIMULINK subsystem

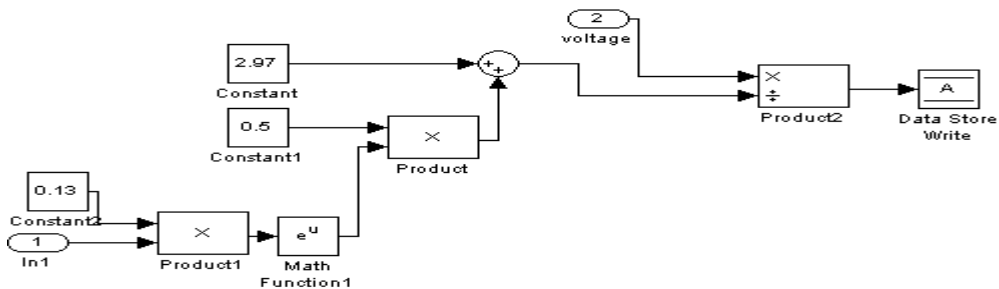
B13.1. Martensite R1



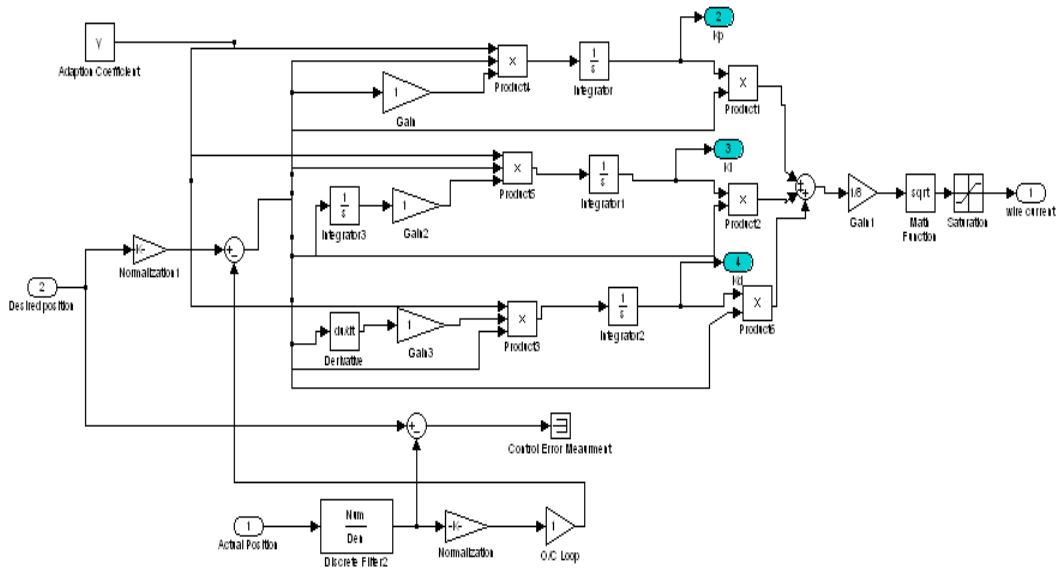
B13.2. Martensite R2



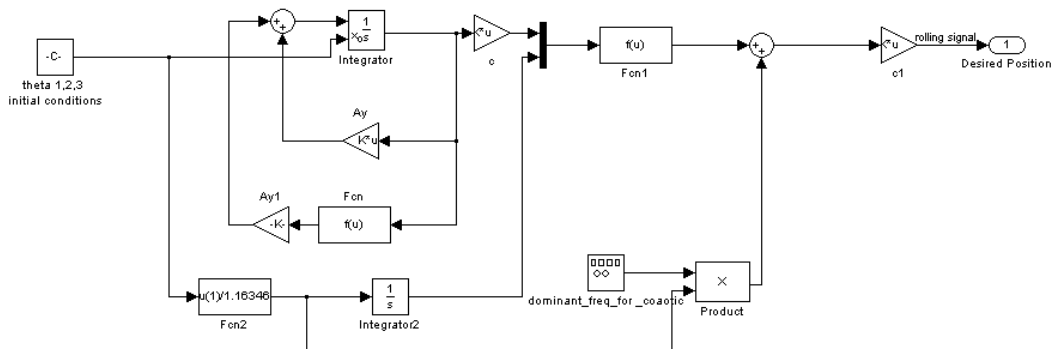
B13.3. Martensite R3



B14. Enhanced PID adaptive controller with error signal as the signal vector of all controller parameters.



B15. Chaotic Signal generator using Chua's equations set.



APPENDIX-C
TABLES AND FIGURES

TABLES

Table C.1. Parameters used in the controller models

Mass (kg)	Cn (F)	h	c (J/KgK)	A (m ²)	V (m ³)	$\delta(\mu\Omega\text{m})$
1,2,3	0.8	150	1350	$4.79 \cdot 10^{-4}$	$6.53 \cdot 10^{-8}$	80

Tables C.2. Discrete Filter Values

Num	$0.6042 \cdot 10^{-3}$	$0.7769 \cdot 10^{-3}$	$0.7769 \cdot 10^{-3}$	$0.6042 \cdot 10^{-3}$
Den	1.0000	-2.7063	2.4541	-0.7451

Table C.3. Transformation Temperatures for the SMA used in the O-Model

As °C	Af °C	Ms °C	Mf °C
38	56	52	36

Table C.4. Effects of desired position frequency on the control error of the PI controller.

Frequency f (Hz)	Kp	Ki	Position Error Range (mm)
0.05	250	20	[-0.2,-0.7]
0.06	250	20	[-0.2,0.5]
0.1	250	20	[-0.42,0.7]
0.2	250	20	[-1.1,1.1]
0.3	250	20	[-2.1,1.3]
0.4	250	20	[-3.2,1.5]
0.5	250	20	[-4.3,2]
1	250	20	[-5.5,1]

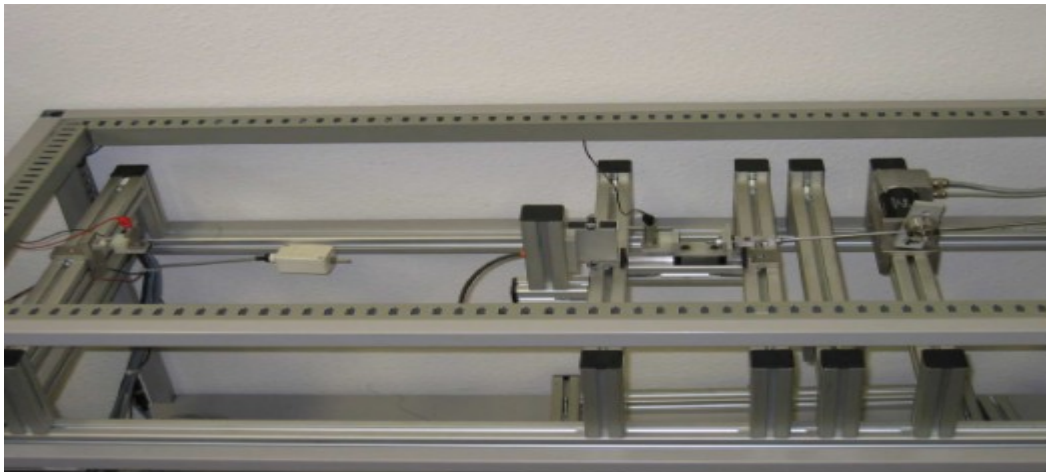
Table C.5. Effects of desired position frequency on the control error of the PID adaptive controller under different set of adaptation coefficients.

Frequency f (Hz)	$\gamma=0.3$ Position Error Range (mm)	$\gamma=0.5$ Position Error Range (mm)	$\gamma=1$ Position Error Range (mm)

0.05	[-0.8,1]	[-0.7,1.1]	[-0.7,1]
0.06	[-2,1.2]	[-0.85,1.0]	[-1,1]
0.1	[-3.4,3]	[-1.7,1.7]	[-1.6,1.6]
0.2	[-3.5,3]	[-3.2,2.9]	[-3.5,2.5]
0.3	[-3.1,3.4]	[-3.2,3.2]	[-3.2,3.2]
0.4	[-3,3.1]	[-3.2,3.2]	[-3.2,3.2]
1	[-4.3,2]	[-3,3.1]	[-3,3.1]

FIGURES

Figure C.1 Experimental Setup at Lab 327/SRS, University of Duisburg-Essen, Germany.



(a) The SMA Test Rig



(b) The removable block



(c) The motor



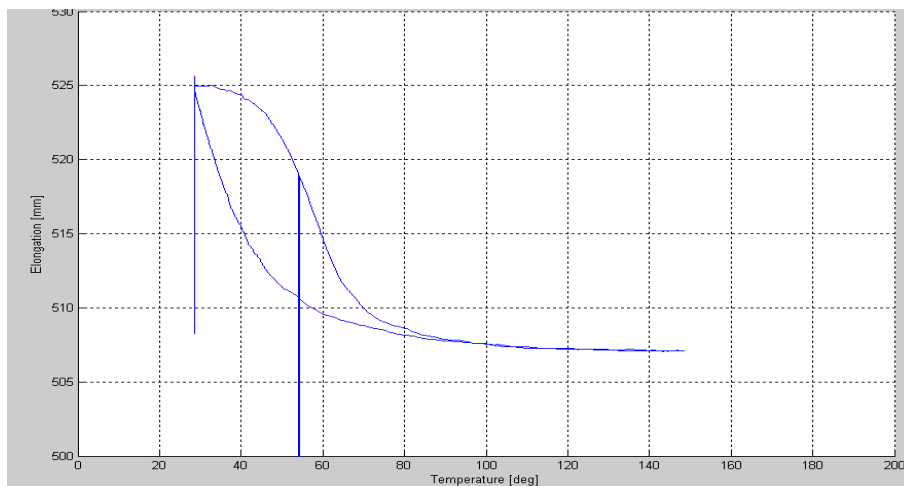
(d) dSPACE control panel



(e) Computer with MATLAB/SIMULINK and dSPACE Hardware and Software

Figure C.2 Hysteresis of the SMA

- (a) Elongation versus Temperature applying one cycle sawtooth current.



(b) Elongation versus Temperature applying sinusoidal input current of 2A amplitude and frequency=0.05 Hz

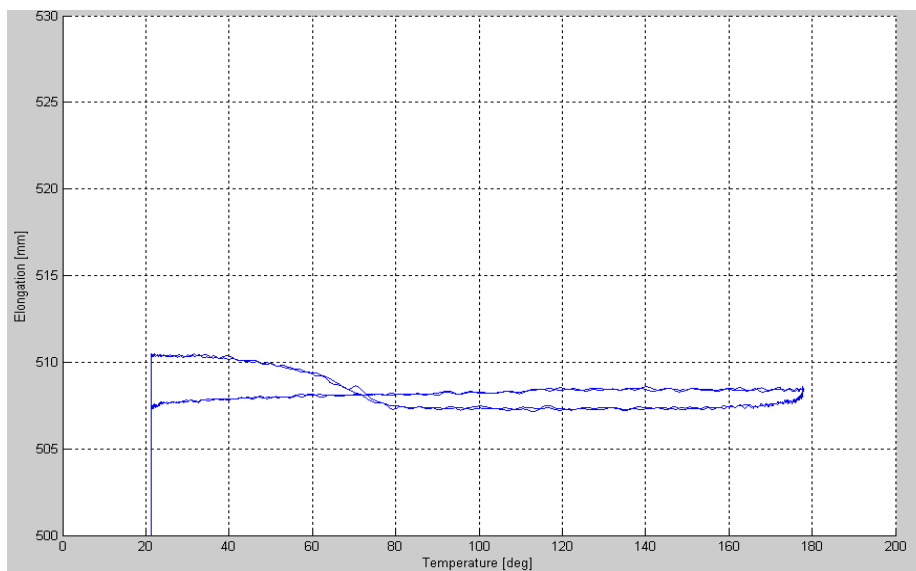
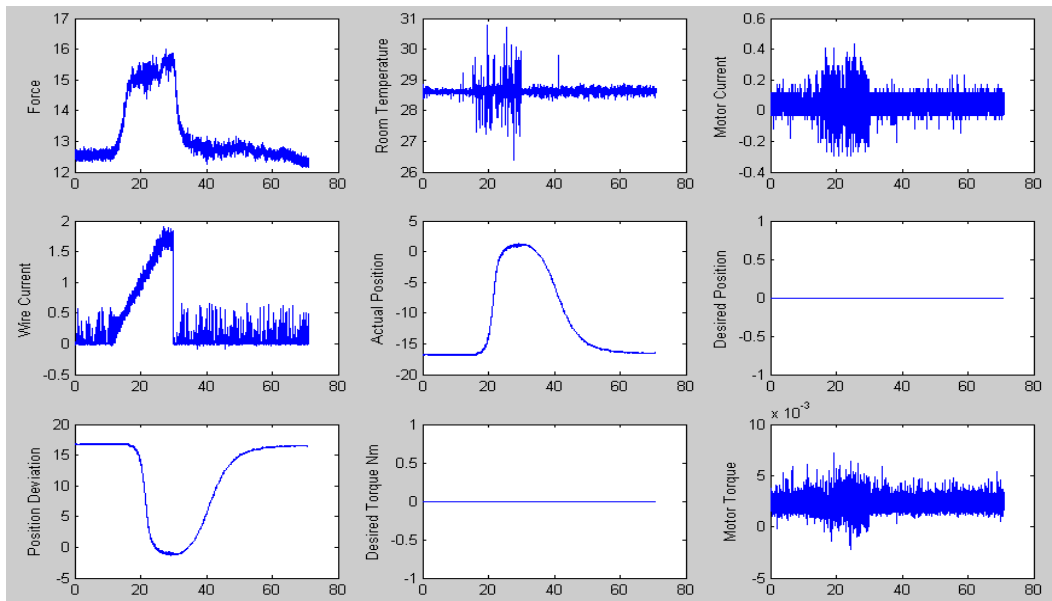


Figure C.3. Test Rig signals

(a) Result of running an experiment on heating-cooling the SMA. Applying one cycle sawtooth current input.



(b) Result of running an experiment on heating-cooling the SMA. applying sinusoidal input current of 2A amplitude and frequency=0.05 Hz

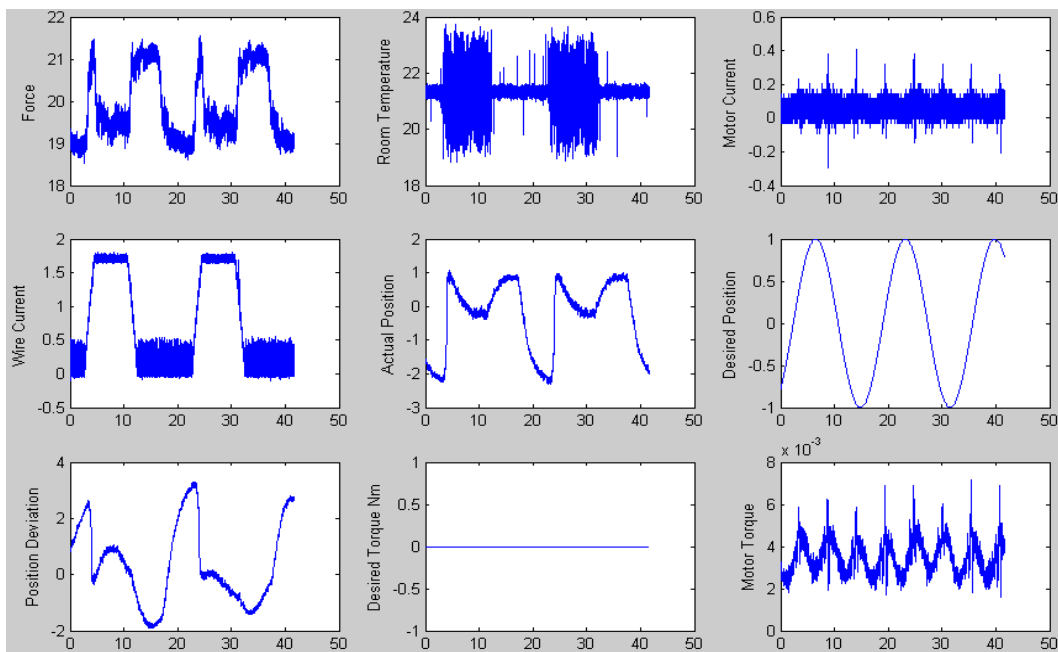


Figure C.4. Snapshot from dSPACE running the experiment of PID adaptive controller as a position controller of the SMA with the error as the signal vector for all controller adaptive parameters.

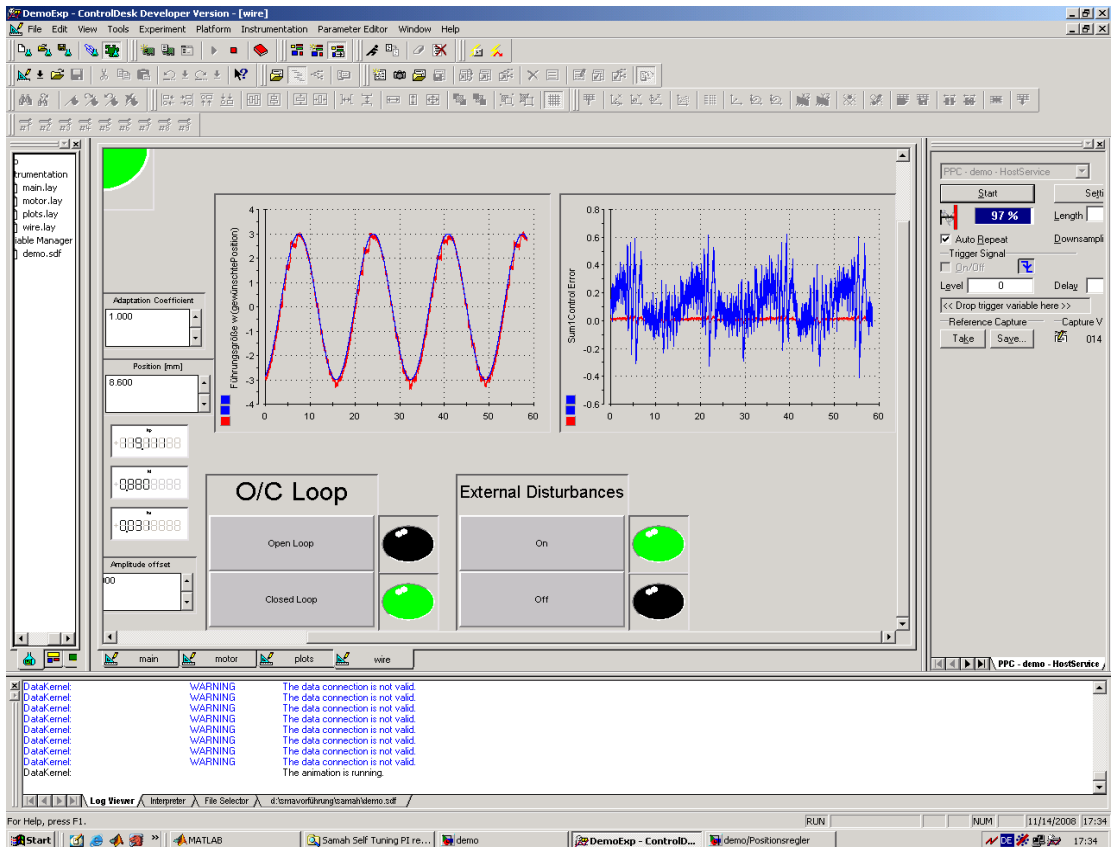


Figure C.4. dSPACE snapshot of the enhanced PID adaptive controller with error as the signal vector. Shows adaptation coefficient $\gamma=1$, controller adaptive coefficients K_p , K_i , and K_d equals 119, 0.88, and 0.031 respectively.

جامعة بير زيت كلية تكنولوجيا المعلومات

التحكم بحركة سلك (Shape Memory Alloy (SMA
باستخدام نماذج أنظمة تحكم مبنية على أنظمة مرتبطة
بالمنظومة الرياضية والأدائية والمنظومة اللاأدائية

أطروحة مقدمة استكمالاً لمتطلبات
درجة الماجستير في الحوسبة العلمية

إعداد

سماح أحمد محمد مصطفى غانم

إشراف

د. حسن شبلي
جامعة بير زيت
رام الله، فلسطين

أ.د. ديرك سوفكر
جامعة دويسبرغ إسن
دويسبرغ، ألمانيا

كانون أول، 2008

ملخص

أسلاك (Shape Memory Alloy (SMA تتصرف بطريقة هستيرية بناءً على قدرتها على تخزين آخر شكل كانت عليه واسترجاعه تحت عمليات التبريد والتسخين الحراري للسلك. الهدف من هذا البحث هو تطوير نظام تحكم حركي لسلك الـ SMA المستخدم كـ actuator.

المجال الأول للتجارب هو اختبار ومحاكاة التصرف الحقيقي لمادة السلك من خلال بناء نماذج تحكم خاصة بذلك. التجارب انقسمت إلى عدة مجالات:

- **أولاً:** اشتقاق نموذج رياضي لطورَي الـ Austinite-Martensite باسم AM-model للمادة باستخدام معادلة التوازن الحراري للمواد، من خلال استخدام طول الـ SMA لإيجاد الموقع الحركي المرغوب به، وذلك عن طريق تعويض معادلة المقاومة الكهربائية للمواد في طور الـ Austinite للمادة. بينما تم فرض حالة من تصرف المادة بجزء فاعل (مواصلة كهربائية) لبناء طور الـ Martensite للمادة. تم اختبار النظام من خلال المقارنة بين الأداء الفعلي للنظام بأداء التجربة، مشكلين نظام تغذية مباشر للتحكم.

- **ثانياً:** اشتقاق نموذج رياضي باسم الـ Volume-model استكمالاً للنموذج الأول أي باستخدام معادلة التوازن الحراري للمواد، مع الأخذ بعين الاعتبار التغير بحجم سلك الـ SMA تحت طورَي الـ Austinite-Martensite خلال التبريد والتسخين للمادة.

- **ثالثاً:** اشتقاق نموذج رياضي باسم الـ Ohm-model لحساب التغير بالمقاومة الكهربائية للسلك خلال الأطوار المختلفة لإيجاد قيم التيار اللازمة لحركة السلك لمواقع معينة. تم اختبار النموذج بنظام تغذية مباشر للتحكم.

كل هذه النماذج لم يتم التأكد من قدرتها الفعلية على تمثيل التصرف للسلك أي التحكم بموقعه بسبب اعتمادها الرئيسي على حساب درجة حرارة السلك. في حين أن درجة حرارة السلك غير متساوية على جميع نقاط السلك السطحية، بينما درجة حرارة السلك المحسوبة بواسطة التقريب للحل العددي لمعادلة التوازن الحراري لا تتوافق مع التغير الحقيقي والسريع لحرارة السلك في الزمن الحقيقي للنظام.

المجال الثاني للتجارب هو اختبار واستخدام أنظمة تحكّم لا تعتمد على خصائص السلك وسلوكه، وذلك باستخدام PI Controller و Adaptive PID Controller. تم اشتقاق واختبار النظامين بنجاح وقد تم التحكّم من خلالهما بحركة سلك الـ SMA بأداء ممتاز. حيث أن نسبة الخطأ قليلة جداً بينما كانت هذه النسبة أعلى تحت ترددات عالية بسبب بطء ردة فعل السلك تحت التبريد الطبيعي.

النتائج المستفادة من البحث:

1. فهم دقيق لقدرات المادة، حيث أن النماذج الرياضية التي استخدمت قد تم اختبارها ببيئة حقيقية أي بتجارب فعلية على النظام و لم تعتمد على الـ Simulation.
2. إيجاد Tuned PI Controller يستطيع التحكم بحركة السلك بشكل دقيق.
3. إيجاد Adaptive PID Controller يستطيع التحكم بأي نظام خطي أو غير خطي و بمتغيرات مجهولة، بحيث يمكن إيجاد متغيرات الـ PID controller بتعبير مبدئي.
4. الفائدة من المجال الثاني للتجارب غير المرتبطة بخصائص السلك وسلوكه هو عدم اعتمادها على درجة حرارة السلك بينما تحتاج هذا النوع من أنظمة التحكم تعبير بسيط من خلال التجارب.
5. من جهة أخرى قدّم هذا البحث قاعدة لتخطيط تطبيقات هندسية باستخدام الـ SMA في مجالات ميكانيكية و كهربائية مثل Smart Antennas والـ Autonomous Systems، الخ...
6. تناول هذا البحث طرح جديد لاستكمال الأبحاث في مجال بناء نموذج للـ SMA لاشتقاق واستنباط نموذج عام يجمع خصائص المادة وسلوكها.

هذا وقد تم استخدام أسلاك الـ SMA من نوع الـ NiTi أو ما يسمى بالنيونول واستخدام برامج الـ MATLAB/SIMULINK ونظام الـ DS1104 و dSPACE لإجراء التجارب.